Channel incision into a submarine landslide: an exhumed Carboniferous example from the Paganzo Basin, San Juan, Argentina

Charlotte Allen [a], Luz E. Gomis-Cartesio [b], David M Hodgson [a,*], Jeff Peakall [a], Juan-Pablo Milana [c]

[a] *School of Earth and Environment, University of Leeds, Leeds, LS2 9JT, UK.*
[b] *Equinor ASA, Rio De Janeiro, Brazil.*
[c] *CONICET-InGeo, Universidad Nacional de San Juan, 5401 San Juan, Argentina.*

**Corresponding author at: School of Earth and Environment, University of Leeds, Leeds, LS2 9JT, UK. Email address: d.hodgson@leeds.ac.uk*

Statement:
This manuscript is a non-peer review preprint submitted to EarthArXiv and has been submitted for review at the open access journal The Depositional Record (https://onlinelibrary.wiley.com/journal/20554877).

Subsequent versions of this manuscript may have different content. If accepted the final version of this manuscript will be available via the 'Peer-review Publication DOI' link on the right hand side of this page, and the White Rose repository: https://eprints.whiterose.ac.uk/

Please feel free to contact any of the authors – we very much welcome constructive feedback.

Twitter handles of authors: @_CharleyAllen - @stratleeds - @hyperpeaknal

Channel incision into a submarine landslide: an exhumed Carboniferous example from the Paganzo Basin, San Juan, Argentina

Charlotte Allen [a], Luz E. Gomis-Cartesio [b], David M Hodgson [a,*], Jeff Peakall [a], Juan-Pablo Milana [c]

[a] School of Earth and Environment, University of Leeds, Leeds, LS2 9JT, UK.
[b] Equinor ASA, Rio De Janeiro, Brazil.
[c] CONICET-InGeo, Universidad Nacional de San Juan, 5401 San Juan, Argentina.

**Corresponding author at: School of Earth and Environment, University of Leeds, Leeds, LS2 9JT, UK. Email address: C.Allen1@leeds.ac.uk*

Abstract

Emplacement of submarine landslides, or mass transport deposits, can radically reshape the physiography of continental margins, and strongly influence subsequent sedimentary processes and dispersal patterns. The irregular relief they generate creates obstacles that force reorganisation of sediment transport systems. Subsurface and seabed examples show that channels can incise directly into submarine landslides. Here, we use high-resolution sedimentological analysis, geological mapping and photogrammetric modelling to document the evolution of two adjacent, and partially contemporaneous, sandstone-rich submarine channel-fills (NSB and SSB) that incised deeply (>75 m) with steep lateral margins (up to 70°) into a 200 m thick debrite. The stepped erosion surface mantled by clasts, ranging from gravels to cobbles, points to a period of downcutting and sediment bypass. A change to aggradation is marked by laterally-migrating sandstone-rich channel bodies that is coincident with prominent steps in the large-scale erosion surface. Two types of depositional terrace are documented on these steps: one overlying an entrenchment surface, and another located in a bend cut-off. Above a younger erosion surface, mapped in both NSB and SSB, is an abrupt change to partially-confined tabular sandstones with graded caps, interpreted as confined lobes. The lobes are characterised by a lack of compensational stacking and increasingly thick hybrid bed deposits, suggesting progradation of a lobe complex confined by the main erosion surface. The incision of adjacent and partially coeval channels into a thick submarine landslide, and sand-rich infill including development of partially confined lobes, reflects the complicated relationships between evolving relief and changes in sediment gravity flow character, which can only be investigated at outcrop. The absence of channel-fills in bounding strata, and the abrupt and temporary presence of coarse sediment infilling the channels, indicates that the submarine landslide emplacement reshaped sediment transport systems, and established conditions that effectively separated sand- from mud-dominated deposits.

1 Introduction

Submarine landslides, or mass-transport complexes (MTCs), and submarine channel systems are common features in deep-water environments, and govern sediment dispersal patterns (Nardin et al., 1979; Piper and Normark, 1983; Pirmez and Flood, 1995). The interaction between mass-transport processes and subsequent submarine channel evolution has been documented in subsurface and modern systems, which have examined i) the formation of canyons through MTC failure (e.g. Nelson et al., 2011), ii) the capture of channel systems within a slide scar (e.g. Bart et al., 1999; Sylvester et al., 2012; Kneller et al., 2016; Qin et al., 2017), iii) the role of MTCs in channel avulsion (e.g. Ortiz-Karpf et al., 2015; Steventon et al., 2021), iv) the initiation and propagation of erosional channel systems above an MTC (e.g. Qin et al., 2017; Zhao et al., 2019; Bull et al., 2020), and v) the influence of MTC topography on planform and cross-sectional architecture of channel-levee systems (e.g. Piper et al., 1997; Moscardelli et al., 2006; Jegou et al., 2008). Seismic reflection data provide information on the large-scale context where submarine channel systems incise into MTCs, but only exhumed systems permit flow-scale evolution and internal architecture to be documented. However, no outcrop studies have examined the interaction of channels that incised directly into an underlying mass-transport deposit (MTD).

Here, we aim to document an MTD that was incised by two channels, exposed in northwest Argentina in a deep-water succession that otherwise has a striking absence of channel-fills. Using detailed, high-resolution sedimentological and stratigraphic analysis, the objectives are to: (i) investigate the evolution of two channels that incise into the MTD; (ii) determine lateral and vertical variations in channel-fill architecture, including terrace deposits, (iii) develop models for channel formation and stratigraphic evolution, and (iv) consider the context of this outcrop in terms of basin-scale processes.

2 Regional context

2.1 Geological Setting

The study area is situated in the western domain of the pericratonic Paleozoic Paganzo Basin and particularly along the Valle Fértil sub-basin where the basin-fill attained a maximum thickness (Fig. 1A; Fernandez-Seveso and Tankard, 1995; Limarino et al., 2002). The tectonic setting remains contentious, with the basin type interpreted as a retroarc foreland basin (Ramos 1988; Limarino et al., 2006), a rift basin (Astini et al., 1995; Milana et al., 2010), a strike-slip basin with elements of extension (Fernandez-Seveso and Tankard, 1995), or as a series of intermittently-linked depocentres, with subsidence linked to subduction (Salfity and Gorustovich, 1983; Ramos et al.,1986; Mpodozis and Ramos, 1989; Fernandez-Seveso and Tankard, 1995). The successions at La Peña and Cerro Bola-Sierra de Maz outcrops are related to subsidence on the Valle Fértil fault, a crustal-scale structure active since Lower Paleozoic times, sometimes as a reverse fault (lower Paleozoic, Milana, 1992; Neogene, Allmendinger et al., 1990) and at other times as an extensional fault (Triassic, Milana and Alcober, 1995). Given along-strike onlap of Upper Paleozoic and Triassic deposits against the Precambrian basement, the Valle Fértil fault could have been extensional, forming a half-graben sub-basin. An interpretation of an extensional setting is supported by basaltic rocks in neighbouring areas dated between 287 and 302 Ma (Thompson and Mitchell, 1972).

The infill of the Paganzo Basin is subdivided into four super-sequences (Guandacol, Tupe, and Upper and Lower Patquia formations) separated by major hiatuses within the Lower Carboniferous to Late Permian (Fernandez-Seveso and Tankard, 1995). The 1800 m thick Guandacol Fm. is subdivided into four depositional sequences, compromising cyclic deposition of fan deltas and basinal turbidites that represent four phases of glacial advance and retreat (Fernandez-Seveso and Tankard, 1995; Valdez et al., 2020). The glacial regime has been interpreted as temperate and wet-based grounded glaciers (Lopez Gamundi and Martinez, 2000; Pazos, 2002), related to local elevations and mountain systems (Limarino et al., 2014) with the generation of large volumes of subglacial sediments (Milliman and Meade, 1983; Elverhøi et al., 1998). An alternative interpretation of glacial regime proposes a large ice sheet located in the continental interior that was drained by long outlet glaciers. The ice-sheet hypothesis is supported by primary glacial deposits identified in the eastern and central Paganzo Basin paleovalley-fills, evidence of a very extensive glacial-valley and fjord system (Milana and Di Pasquo, 2019, and refs therein), and the paleogeomorphological study of paleovalleys within the continental interior that support the presence of outlet glacier valleys (Valdez Buso et al., 2021). This model explains the almost complete absence of primary glacial deposits in the continental interior, their widespread presence in coastal areas (the Precordillera), and the large volumes of proglacial sediments (cf. Eyles et al., 1985). The area of La Peña is interpreted as an alternating proglacial/non-glacial, irregularly-shaped submarine slope system with kinematic indicators in successive mass-transport deposits (MTDs) that support the presence of an overall north-facing slope, but with a spread of transport directions from NE-to-WNW (Milana et al., 2010; Sobiesiak et al., 2017; Valdez Buso et al., 2019).

2.2 Study location

This study focuses on large exposures in the modern day La Peña river valley within the Ischigualasto Provincial Park, on the border of San Juan and Rioja provinces, northwestern Argentina (Fig. 1). The modern-day river valley incises into the western flank of the Ischigualasto and Caballo Anca ranges, part of an uplifted basement block related to the crustal scale Valle Fertil fault (Valdez Buso et al., 2019). The study area is cut by a number of northwest-southeast trending oblique normal faults, forming a horst structure in the central part of the study area (Figs. 1D, 2A-C).

Five thick (150-220 m thick) MTDs intercalated with packages of mud- to sand-prone turbidites, form ~900 m of stratigraphy, overlain by sand-prone turbidites (Fig. 1C), as part of the Guandacol Formation (Sobiesiak et al., 2017; Valdez Buso et al., 2019). The Carboniferous succession is irregularly eroded and overlain by the lower Triassic red beds of

Tarjados and Talampaya formations. The base at the Carboniferous section is not exposed, but 3 km to the SSE of La Peña gorge the lower Carboniferous units onlap crystalline basement.

Our study focuses on a c. 250 m thick section of the Guandacol Formation at La Peña that is marked by a basal >200 m thick silt-prone MTD, with an erosive base and megaclasts (10s m diameter), termed MTD 5 (Milana et al., 2010; Valdez Buso et al., 2019). Underlying MTD 5, the stratigraphy is characterized by a dark mudstone unit with thin bedded tabular turbidites, suggesting a distal setting. The top of MTD 5 is reasonably flat at the scale of the outcrop, and is only locally incised by the submarine channels described herein. About 10 meters above MTD 5 is a ~7 m thick, deformed sandstone-rich unit characterised by imbricate thrusts, named MTD 6 (Milana et al., 2010; Valdez Buso et al., 2019). Overlying MTD 6 are tabular sandy turbidites arranged in packages, suggesting stacking of lobes in a lobe complex (*sensu* Prélat et al., 2009). While MTDs 1 to 4 were deposited in a proglacial environment, there is no indication that MTDs 5 and 6 had proglacial influence (Valdez Buso et al., 2019). The pre-conditioning for the submarine landslide is linked to the thick mudstone underlying MTD 5, which contains a maximum flooding zone that formed during deglaciation (Cycle 3 of Valdez Buso et al., 2020).

Two outcrops form the focus of this study: 1) La Peña outcrop (Figs. 1, 2A-C), trending NE-SW, comprising two sandstone bodies with erosional bases. The largest, to the south, herein termed the Southern Sandstone Body (SSB), is 400 m wide and ~75 m thick (Fig. 2B). The Northern Sandstone Body (NSB) is ~350 m wide and ~60 m thick (Fig. 2C), separated from the SSB by a horst block (Figs. 1, 2B-C). 2) The La Charca outcrop (Figs. 2E-F, E and F on Fig 2A), 2.5 km to the southeast, is described in this study using outcrop models and satellite imagery. Previous authors have interpreted these outcrops as recording ponded turbidites above topographic lows of the MTD (Kneller et al., 2016; Valdez Buso et al., 2019).

2.3 Methodology

Eleven high-resolution (centimetre-scale) composite sedimentary logs and numerous shorter logs were measured to document lithology, grain-size variation and sedimentary structures (total measured thickness: 363 m; Figs. 3, 4, 5). Key stratal boundaries were identified at outcrop (Fig. 2B), registered on a detailed geological map (Fig. 1) and aerial photographs, and in combination with the logs, used to establish a correlation framework using lateral and vertical lithofacies relationships (Figs. 1, 4, 6). Palaeocurrent data (n = 291) were collected from ripple and climbing ripple cross-lamination, grooves and flutes, and orientation of erosion surfaces (Figs. 4, 6).

3 Facies groups

Five facies associations have been identified and grouped based on interpreted processes and depositional environment.

3.1 Facies association 1: Remobilised deposits

(A) Megaclast-rich poorly sorted deposit

Description: Heterogeneous packages up to 70 m thick (Fig. 3A) with pale yellow medium sandstone clasts, ranging from mm-scale stringers to >50 m diameter. The basal surface cuts step-wise into underlying sandstone turbidites by up to 5 m, and is immediately overlain by gravel layers (Valdez Buso et al., 2019). The concentration of clasts varies laterally and vertically, with zones of both clast- and matrix-supported fabric, and an upward transition into matrix-supported dark green-grey, poorly-sorted siltstones with gravels and pebbles as layers and as isolated clasts (FA1B). Locally, clasts have sheared margins, exhibit internal contortion, and preserve a range of disaggregation states. FA1A and FA1B share the same process interpretation (below) and were deposited as a single event.

(B) Siltstone-rich poorly-sorted deposit

Description: Comprises homogeneous, dark green-grey, poorly-sorted siltstone matrix (Fig. 3B), with rare pebbles and cobbles, and gravels dispersed throughout, with a range of extra- and intra-basinal igneous, metamorphic and sedimentary lithologies. Commonly, sandstone clasts show evidence of shearing. Siltstones are folded and sheared, and locally cut by surfaces with abrupt changes in orientation. The boundary between siltstone and overlying sandstone also exhibits loading, and wave-like geometries (Fig. 3B). FA1B can be up to 150 m thick.

Interpretation: The stepped basal surface, and evidence of shearing distributed throughout the deposit, and a matrix-supported and deformed fabric in the upper section, support interpretation of a debrite (Dott, 1963; Nardin et al., 1979; Moscardelli et al., 2006) emplaced in a single event that cut into the substrate. Previous authors have interpreted overpressure of pore fluids and hydroplaning along gravel layers at the base of the debris flow as a mechanism for emplacement (Valdez Buso et al., 2019). The upper contact of FA1B is characterised by soft-sediment deformation and interpreted to indicate local liquefaction and fluidisation, cut by sandstone injectites.

(C) Sandstone-rich deformed deposit

Description: FA1C is a heterolithic deposit comprising medium yellow-grey sandstone beds (0.15-0.3 m thick), interbedded with siltstone layers, overlain by a 0.3 m thick medium sandstone with siltstone clasts distributed throughout. The overlying package (0.5 to 5 m thick) comprises grey-yellow-orange, medium to coarse structureless sandstones, with rare small pebbles and gravels dispersed throughout. Laterally, the structureless sandstone transitions into blocky, imbricated sandstone sheets (Fig. 3C) that comprise two sets of thrust fault planes that dip ~25°.

Interpretation: The lateral variation in thickness and disaggregation is consistent with interpretation of FA1C as a slide (MTD 6 of Milana et al., 2010; Valdez Buso et al., 2019) from remobilisation of a sandbody, with toewall buttressing resulting in imbricated thrusts.

3.2 Facies association 2: Axial channel-fill

(A) Pebbly sandstones and conglomerates:

Description: Erosive, laterally discontinuous, undulose, lensoidal beds (0.1-0.8 m thick) bounded by erosion surfaces overlie the deepest point of a composite erosion surface (>75 m of incision into FA1), showing a high degree of lateral and vertical thickness and facies variations. The beds show highly variable proportions of clast: matrix, with beds varying from clast-supported to matrix-supported. Matrix-supported beds consist of poorly-supported, granule to cobble clasts with a wide range of rock types and shapes, from rounded to angular (Fig. 3D), supported by a dark grey-brown, poorly-sorted, medium to coarse sandstone and white granule matrix with abundant siltstone rip-up clasts. Clast-supported beds have a smaller range of clast sizes, from granule to large pebble, with a coarse sandstone matrix. Grooves (0.1 m deep) are present on the base of matrix-supported beds.

Interpretation: Lenticular, clast-supported pebbly sandstones bounded by erosion surfaces are interpreted as lag deposits, with clasts carried as bedload transport (Mutti and Normark, 1987; Mutti, 1992). Poorly-sorted, matrix-supported, clay-poor beds suggest deposition from a debris flows (Mutti et al., 2003), with the presence of grooves further indicating passage of cohesive flows, such as debris flows or slumps (Peakall et al., 2020). The position of these lag deposits associated with the composite erosion surface supports the interpretation that FA2A formed through the passage of multiple erosive flows that formed a sediment bypass-dominated zone (Winn and Dott 1977; Mutti and Normark, 1987; Gardner et al., 2003; Beaubouef et al., 2004; Stevenson et al., 2015).

(B) Amalgamated sandstone beds:

Description: Homogeneous, erosively-based sandstone beds (0.5-~4 m thick), with common amalgamation surfaces, comprising white-grey, angular to sub-angular, medium- to well-sorted, very coarse sand and granules (Fig. 3E) that stack to form laterally extensive packages. Typically, beds are structureless with weak normal grading and planar lamination at bed tops. Bed bases occasionally exhibit large, wide flute casts and weakly stratified siltstone clast-rich units that form discrete layers, and some beds contain dish structures.

Interpretation: Thick, clean sandstones deposit under high-density turbidity currents and sandy debris flows (Bouma, 1962; Lowe, 1982; Mutti, 1992; Kneller and Branney, 1995; Talling et al., 2012). The alignment of siltstone clasts and presence of flute casts on the base suggests formation from turbidity currents, as opposed to *en masse* deposition (Kneller and Branney, 1995; Talling et al., 2012; Peakall et al., 2020). Furthermore, flute geometry suggests deposition in a proximal environment (Pett and Walker, 1971; Peakall et al., 2020). Structureless sandstones within the succession can result from deposition from a steady, uniform current (Kneller and Branney, 1995), which may be sufficiently rapid to induce liquefaction (Lowe, 1982; Kneller and Branney, 1995; Peakall et al., 2020) precluding the development of depositional bedforms (Lowe, 1982).

(C) Normally graded sandstone beds:

Description: Beds with lateral thickness variations (0.3 - 2.5 m thick) have erosional bases, and comprise well-sorted, structureless, normally graded, white-grey very coarse sandstone, with granules dispersed throughout, and dish and flame structures. Commonly, there is an abrupt grain-size break to a fine-grained planar and ripple laminated sandstone and siltstone division (Fig. 3F).

Interpretation: Very coarse, structureless sandstones were deposited by high density, sand-rich turbidity currents (Lowe, 1982). Dewatering structures form through liquefaction (Mulder and Alexander, 2001; Stow and Johansson, 2002) likely related to rapid deposition (Lowe, 1982; Peakall et al., 2020). Finer grained material was deposited from low-density turbidity currents, with tractional structures formed from reworking by dilute flows above the bed (Allen, 1984; Southard, 1991; Best and Bridge, 1992). The grain-size break is interpreted to reflect the transition from high to low density turbidity current deposition (Sumner et al., 2008), and may indicate sediment bypass (Stevenson et al., 2015).

3.3 Facies association 3: Terrace deposits

(A) Fissile thin-beds

Description: Primarily comprises relatively continuous fissile beds (<2 cm to mm thick) of fine siltstone to fine sandstone (Fig. 3G), with no clear lateral or stratigraphic bed-thickness or grainsize trends (Figs. 5B-C). Thicker beds exhibit asymmetric 'micro-ripple' lamination (<1 mm amplitude, ~5 mm wavelength) on the upper surface of coarse siltstones. Bed bases and tops are sharp, with little evidence of erosion into underlying beds.

Interpretation: Deposition from upper, dilute parts of turbidity currents (Lowe, 1988). Thin beds suggest low suspension fall out rates. The micro-ripples on the tops of beds are the product of very early stage (incipient) ripples in silts (Rees, 1966; Mantz, 1978), suggesting limited time for tractional reworking and thus a rapidly waning flow.

(B) Scoured thin-beds

Description: Undulating, fine to coarse, well-sorted sandstone beds with erosive bases, which are commonly truncated by scour surfaces (Fig. 3H). Thinner beds are normally graded, and thicker beds show little grain-size variation, with rare basal siltstone chips (0.5-1.5 cm diameter). Typically, beds of coarser grainsize exhibit cross ripple lamination along with granules dispersed throughout beds that can follow ripple foresets, and finer-grained beds exhibit parallel lamination. Scour-fills are concentrated in granules, and contain siltstone clasts and rare inclined laminae sets.

Interpretation: Deposition and tractional reworking by upper dilute parts of turbidity currents (Lowe, 1982). The presence of abundant scour surfaces, infilled by granules indicates sediment bypass, and suggests deposition at a relatively low elevation with respect to the active channel (Hansen et al., 2015). Normal grading and tractional structures overlying these surfaces suggest formation by low-density turbidity currents (Lowe, 1988; Kneller and Branney, 1995).

3.4 Facies association 4: Lobe environments

(A) Tabular beds

Description: Metre-thick tabular beds with limited basal erosion comprised of white-grey, angular to sub-angular, medium- to well-sorted, coarse sandstone and granules. Beds are weakly normally graded, with rare parallel and current ripple laminations at bed tops and rare isolated siltstone clasts in bed bases. Bed contacts are amalgamated or separated by a defined erosion surface.

Interpretation: Normally graded sandstones are interpreted to form from high-density turbidity current deposition (Bouma, 1962; Lowe, 1982; Talling et al., 2012), with tractional structures formed by reworking of the bed by dilute flows (Allen, 1984; Southard, 1991; Best and Bridge, 1992). Weak normal grading and planar lamination indicate deposition from a waning current (Kneller and Branney, 1995).

(B) Sandstone-siltstone thin-beds

Description: Beds (1-30 cm thick) comprise a basal dark yellow, medium-grained sandstone division and an overlying dark grey-black fine-grained siltstone division (Fig. 3I), with siltstone often thicker than the sandstone. Sandstone divisions have erosional bases, are tabular, and commonly exhibit weak planar and rare current ripple lamination (Fig. 3J). Typically, siltstone divisions are finely-laminated, lack grading, and are thicker than the underlying sandstone layer. Some beds exhibit a sharp grain-size change from sandstone to siltstone, with some normally graded from sandstone to siltstone within 2 cm.

Interpretation: Structureless sandstones suggest high-density turbidity currents. The nature of the contact between the sandstones and the overlying siltstones indicates two different processes. Beds with an abrupt transition from sandstone to siltstone division are interpreted as a function of density stratification within the flow (Kneller and McCaffrey, 1999), or as a result of bypassing of the transitional grain-size faction (Stevenson et al., 2015). In contrast, beds with grading from sandstone to siltstone divisions suggest trapping of turbidity currents (Sinclair and Tomasso, 2002), which were unable to surmount a down-dip obstacle.

(C) Bipartite debrite-sandstone beds

Description: Bipartite beds (0.3 – 0.8 m thick) comprise a lower, moderately well sorted coarse to medium sandstone division, and an upper poorly-sorted silty-sandstone division (Fig. 3K). The lower division is characterised by erosive bases and is structureless with siltstone rip-up clasts, dispersed throughout. The upper division is matrix-supported, poorly-sorted silty–sandstone with dispersed medium and coarse sand grains, and siltstone-clasts (0.1-6 cm diameter). Larger siltstone clasts are located in the lower bed division and are elongated, with sub-angular to rounded edges, whilst smaller clasts (<2 cm diameter) are dispersed throughout. The contact between divisions is diffuse.

Interpretation: The lower sandstone division is interpreted as a high-density turbidite (Lowe, 1982; Talling et al., 2012). The overlying silty-sandstone with clasts dispersed throughout, is interpreted as a debrite, which is genetically linked to the underlying turbidite, with the bipartite beds interpreted as hybrid beds (Haughton et al., 2003; 2009; Talling et al., 2004).

3.5 Facies association 5: Lobe-fringe deposits

Description: Beds (0.05 - 0.2 m thick) of sharp-based, dark red-brown to dirty yellow, well-sorted medium sandstone with an abrupt transition to thick (up to 0.75 m, compared with 0.2 m sandstone) coarse siltstone (Fig. 3L). Sand grains are sub-rounded to rounded, and beds contain a high proportion of mica. Beds exhibit abundant planar, ripple and climbing ripple lamination. Normally, graded sandstone beds are interbedded with 0.3-0.85 m thick packages of coarse siltstone, exhibiting parallel lamination and occasional cm-scale medium to coarse sandstones. The thickest exposure (upper part of Log 3, Fig. 4) shows a coarsening- and thickening-upwards succession, passing vertically from siltstones interbedded with cm-scale medium-coarse sandstones, to medium sandstone beds up to 0.2 m thick and thin siltstones. Rare sharp or erosively-based siltstone clast-rich medium sandstone beds (0.2-0.4 m) are present in the SW close to the boundary with FA1A. Clasts are disseminated throughout beds, with no evident stratification or grading, with bed bases occasionally exhibiting grooves. Rare, isolated wood fragments are found on bed contacts.

Interpretation: Tractional structures formed through deposition from, or reworking by, low-density turbidity currents (Talling et al., 2012), with climbing ripples indicating rapidly decelerating flows (Jobe et al., 2012). The abundant mica and the presence of wood suggest a direct terrestrial source, and in turn hyperpycnal flows (Zavala and Pan, 2018). Additionally, basal grooves suggest bypassing of debris flows, or a debritic flow component (Peakall et al., 2020), and deposition of beds with chaotically-distributed clasts and no grading is indicative of debrites (Talling et al., 2012).

4 Stratigraphic framework, architecture and depositional elements:

The succession at La Peña is subdivided into four units (Units 1-4), with Unit 2 further divided into 4 stratigraphic packages (only present in the SSB; Fig. 4), based on lithology, facies, bed geometry and bounding surfaces.

4.1 Unit 1 - Debrite

Unit 1 (~200 m; Fig, 4) is MTD 5 of Milana et al. (2010) and Valdez Buso et al. (2019), and comprises ~70 m of FA1A and ~130 m of FA1B, with an erosional base, cutting step-wise into underlying turbidites by up to 5 m (Figs. 2A, 3A). Megaclasts at the base are up to 50 m wide and 7 m high, and are in contact with each other. The megaclasts decrease in size and number upwards into the matrix-supported upper part of MTD 5 (Figs. 1C, 3A). The poor sorting and matrix-supported megaclasts support interpretation of a debrite.

4.2 Surface 1 (S1) – Erosion surface

In the Southern Sandstone Body (SSB) area, MTD 5 is cut by a >75 m deep, 400 m wide concave-up surface, with stepped margins to the SW and NE (Fig. 4). The SW margin steepens with height (maximum 70°) and exhibits an uneven geometry, before passing westwards to an irregular surface that flattens to sub-horizontal (Figs. 1, 4). This surface is also characterised by clastic dykes marking sand injection into the underlying debrite. The

NE margin is faulted (Figs. 1, 2A), with the exposure of S1 on the uplifted block sub-horizontal (Figs. 2B-C); the lower portion of this margin is inferred to be a similar gradient to the SW margin. Surface 1 in the Northern Sandstone Body (NSB) area is characterised by smooth margins (to the W and NE). The W margin is steeper and faulted, and the NE margin is more rugose (Fig. 2C). Grooves and other tool marks are present on S1, with depths of up to 0.15 m and a greater width than depth. Palaeoflow from grooves in S1 range from 130/310°-174/354° in SSB, and 108/288°-143/323° in NSB). Pebbles are occasionally present in the base of the tool, suggesting they were the tool-makers. These grooves were likely cut by bypassing flows with cohesive strength such as debris flows, slumps, or the debritic component of hybrid beds (Peakall et al., 2020). Immediately overlying S1 are the lenticular conglomeratic beds of FA2A, interpreted as lag deposits, present on the stepped surfaces and the lowest point of S1. The stepped geometry, and indication of sediment bypass at different stratigraphic levels, suggest Surface 1 is a composite erosion surface that deepened through time (cf. Hubbard et al., 2014; Hodgson et al., 2016).

4.3 Unit 2 – Southern Sandstone Body area

4.3.1 Package 1 (P1) – Initial bypass and infill

Package 1 (P1; ~20 m thick) directly overlies the lowermost part of S1 in the SSB (Fig. 4) and comprises a laterally discontinuous basal conglomerate (up to 3 m thick; FA2A), with overlying tabular, commonly amalgamated, very coarse-grained sandstone beds (~17 m thick; FA2b). Multiple erosion surfaces separate FA2A and FA2B, suggesting a phase dominated by sediment bypass. FA2B is present up to the first step in S1 to the SW, where beds onlap S1 at an angle of ~20°. Flute casts on the base of a P1 bed indicate palaeoflow ranges from 265-040°, but predominantly to the NW (Fig. 4). Towards the top of P1, a thin (0.2 m thick) partially preserved unit of ripple laminated fine sandstones (palaeoflow range 140-040°) and coarse siltstones is interpreted to represent a period of reduced sediment supply. The sand-rich, commonly amalgamated deposition from high-energy flows, and location within an incisional confining surface (S1) supports interpretation of these deposits as axial channel fills.

4.3.2 Package 2 (P2) – Aggrading channel-fills

In general, Package 2 has a higher proportion of fine-grained material, siltstone clasts, and thinner beds than P1. FA2C dominates P2, and thickens from 3 m in the east to 16.5 m above the deepest point of Surface 1, then thins to 6 m in the SW (Fig. 4). P2 is subdivided by the geometry and lateral extent of beds (Fig. 4) into lower P2 and upper P2. Lower P2 is characterised by southward-thinning beds (from ~9 m to 2.5 m; fig. 4) extending across the channel cut; to the east, the base of lower P2 directly overlies S1 (Fig. 2B, D) and further west it overlies Unit 1 (Figs. 2B, 4). Lower P2 is also correlated to the sandstone exposure on top of the horst block to the north (Figs. 2B, 4). This exposure of P2 can be traced northwards across the horst block (Fig. 2C) and correlated with an erosion surface overlying confined heterolithic deposits (T1) in the north (Fig. 1). The base of P2 in contact with S1 and Unit 1 indicates the presence of a palaeo-high during deposition, or a stepped geometry of the NE margin above the level of P1 deposition. Groove data from S1 on the horst block gives palaeoflow readings of 092/272°-172/352°. Above this, lower P2 thins westward from ~9 m to 2.5 m thick, whilst on the eastward side it is cut by the basal surface of P3 (Fig. 4). Upper P2 exhibits multiple concave-up erosion surfaces bounding laterally discontinuous bodies of sandstone-rich deposits (FA2C; Fig. 4), interpreted as smaller-scale channel cuts within the larger-scale S1.

The thickest part of upper P2 is to the west. The component beds are more lenticular, with erosion surfaces defining channelised bodies ranging from 1.5-4 m thick. These exhibit a highly aggradational stacking pattern, with limited lateral offset to the east (Fig. 4). Palaeocurrent measurements taken from ripple cross laminations in finer-grained bed caps have a wide range of directions throughout the stratigraphy (062-326°) (Fig. 4), most likely indicating flow deflection from surrounding topography (e.g. Kneller et al., 1991).

4.3.3 Package 3 (P3) – Channel widening

The base of Package 3 is erosional, and is coincident with a widening of the SSB, marked by a prominent step in Surface 1 on the SW margin (Fig. 4). Because pebbly sands and conglomerates (FA2A) are only present overlying S1 on the step, and not associated with P3 within the channel cut, the step is interpreted to have formed during the initial formation of S1. P3 is ~11 m thick and comprises the same tabular, amalgamated sandstone facies (FA2B) as P1, with no fine-grained bed caps (Fig. 4). It is not possible to identify the lateral and vertical extent of P3 in the SW of the SSB, due to exposure limitations. However, bed thickness, degree of amalgamation, and lack of fine-grained material suggest that flows were still channelised at this point.

4.3.4 Package 4 (P4) – Transition from confined to weakly-confined.

Package 4 is the most laterally extensive in the study area, and is present in the SSB and NSB (Fig. 4). The base of P4 is marked by an irregular erosion surface (Surface 2 (S2)), overlying P3 and off-axis deposition to the SW (Fig. 4). S2 incises up to 2 m in the east, but the geometry to the SW is unknown, due to exposure limitations. In Log 4, the surface is marked by an A scour infilled with mud-clast-rich FA2A marks S2 at Log 4, indicating the passage of, and deposition from, debris flows (Peakall et al., 2020). P4 (~22.5 m thick) coarsens and thickens upwards (Fig. 5), and comprises five distinct, laterally variable but tabular sandstone beds and bedsets of FA4A (herein named L1-5), intercalated with packages of thin-bedded sandstones and siltstones (FA4B). The upper stratigraphy is characterised by hybrid beds (FA4C), which are commonly found in distal lobe fringes (e.g. Hodgson 2009; Spychala et al., 2017a, c), although hybrid beds are also observed in proximal environments, where the debritic component may be sand-rich (e.g., Fonnesu et al., 2015; Brooks et al., 2018). L1-L5 are dominated by a thick sandstone bed, and in the case of L1 and L5, amalgamated sandstones (Figs. 4, 5). Together with the overlying thinner beds, these are interpreted as lobe elements, collectively forming a single lobe (*sensu* Prélat et al., 2009) confined within S1, marking an abrupt stratigraphic change from channelised to lobe deposition.

In the lower stratigraphy of P4, ripple current lamination record palaeocurrents ranging from 134-352°, and together with the pronounced normal grading of beds from sand to silt, suggests flow deflection off, and trapping of flow by, topography downstream (e.g. Sinclair and Tomasso, 2002, Hodgson and Haughton 2004). L1 and S2 are cut by a high angle (~45°) erosion surface (Fig. 5) that is overlain by ~3.5 m of interbedded sandstones and siltstones (0.1-0.5 m thick), and is interpreted as a scour-fill (Fig. 4).

L4 is continuous across the outcrop and amalgamates with L3 eastwards (Figs. 1, 4, 5). In the central SSB area and westward, L3 and L4 are separated by a package of hybrid beds, reaching a maximum thickness of 5 m. L3 and L4 onlap the western margin. The upper part of P4 comprises laterally continuous package of hybrid beds (4 m thick), overlain by L5 (~3-7 m thick). Palaeocurrents within the lower package of hybrid beds range from 026-332° and show a 360° range in the upper package (Fig. 4), further supporting flow deflection and reflection in the upper package of hybrid beds.

4.4 Unit 3 – Overlying turbidites (FA5) – Lobe fringe deposits

Unit 3 is correlated from the SSB to the NSB to form a high aspect ratio package (Fig. 1). The contact between Unit 2 and Unit 3 (FA5) is characterised by an abrupt transition from thick-bedded and amalgamated coarse sandstones (L5) to coarse siltstones (Fig. 4). Unit 3 forms a 2-5 m thick coarsening- and thickening upwards package from siltstones interbedded with cm-scale sandstones to increasingly thick (up to 10 cm) sandstone beds (Fig. 4). Palaeocurrents from current ripple lamination range from 020-080°NE, with grooves averaging 080-260°. Commonly, thin-bedded, rippled sandstones in tabular packages are interpreted as lobe fringe deposits (e.g. Prélat et al., 2009; Marini et al., 2016; Kane et al., 2017; Spychala et al., 2017a). The absence of hybrid beds suggest flows did not transform because they were not able to entrain a muddy substrate. The thickening upwards supports a transition from distal lobe fringe to lobe fringe, and progradation of the system.

4.5 Unit 4 – MTD 6

Unit 3 is overlain by MTD 6 (up to 7 m thick; Figs. 1, 3C) in both the SSB and the NSB, transitioning from massive sandstone beds, to an imbricated thrust complex with pop-up sand blocks in the NE of the NSB supporting interpretation of a slide. Previous authors have determined palaeoflow to the NE, based on orientation of thrust faults within the slide (Sobiesiak et al., 2012).

4.6 NSB fill

The NSB-fill is up to 60 m thick (Fig. 6), with 2 m of lenticular, conglomeratic beds (FA2A) overlying S1. Above this ~40 m of very coarse sandstones (0.4 to ~3 m thick; FA2B) is present that thin and become less amalgamated towards the margins. The presence of high-density turbidity current deposits confined by S1 supports an interpretation of axial channel sandstones. Above this, S2 is overlain by a 0.2 m thick, laterally-discontinuous bed of FA2A in the east (Fig. 6). P4 (L2-L5) of Unit 2 is correlated from the SSB, with Units 3 and 4 also present overlying the NSB. P4 has a similar stacking pattern, with four distinct sandstone beds (FA4A) intercalated with FA4B and FA4C. FA4B is present in the central part of the outcrop, with a 360° spread of palaeocurrents, but absent to the NE. L2 to L4 are tentatively correlated across the area. L5 and Unit 3 were walked out and correlated across faults using their distinctive lithology and bed architecture. Unit 3 (~3 m thick) contains palaeocurrents ranging from 357°-084°. Overall, P4 thins and onlaps towards the NE margin of MTD 5, before passing into the subcrop (Fig. 1).

4.7 Off-axis deposition on elevated surfaces

Three distinct sedimentary successions overlie steps in Surface 1, with one between the NSB and SSB (T1) (Fig. 1) and the others on small (10 m-wide) concave-up steps (T2 and T3) to the west of the SSB (Figs. 1, 4). These deposits share similar depositional architectures and processes.

4.7.1 T1

T1 is located between the SSB and NSB, is ~15 m thick, and directly overlies S1 and MTD 5, (Figs. 1, 7A-C). T1 primarily comprises fissile thin-beds (FA3A), with rare 0.05-0.1 m thin-beds (FA3B) exhibiting minor erosional bases (Figs. 7B-C). Palaeocurrent measurements from current ripple lamination range from 040-340°. Deformation and rotation of T1 deposits towards the SW indicates post-depositional sliding toward the axis of the NSB (Fig. 7A). The rotated and deformed T1 deposits are cut by a SSW-NNE orientated erosion surface (~20° dip) (Fig. 7A), overlain by a 0.75 – 1.2 m thick sandstone bed (FA2B). Grooves on the base of the sandstone (palaeoflow range 070/260°-100/280°) indicate passage of debris flows over the surface (Peakall et al., 2020). This sandstone bed can be traced laterally to the west across the horst block, where it overlies MTD 5, and is correlated across a fault, to the base of P2 in the SSB outcrop (Figs. 1, 2A-C). This indicates that the deposition, deformation, and erosion of T1 occurred prior to the deposition of P2 within the SSB.

4.7.2 T2

T2 (24 m thick; Figs. 1, 4) is located to the SW of the SSB, and is underlain by a package of conglomerates and pebbly sandstones (FA2A) that overlie S1, and are interpreted as deposits from a bypass-dominated phase. T2 comprises two discrete sections; the lower section (~5 m thick) comprises 0.1 – 0.8 m thick packages of scoured thin-beds (FA3B), and the upper section (~3 m thick) comprises fissile thin-beds (FA3A). T2 is cut by S2 (Fig. 4).

4.7.3 T3

T3 is the thickest deposit of this type (~32 m; Figs. 4, 7-8). The lower part of T3 overlies a package of pebbly sandstones and conglomerates (FA2A, 0.4-0.8 m thick) that overlie S1, which are interpreted as bypass-dominated deposits. The overlying T3 stratigraphy is subdivided into a lower and upper succession (Fig. 8). Lower T3 comprises six 1-3 m thick coarsening- and thickening-upwards units (T3.1-3.6) of fissile- (FA3A; Fig.

7D) and scoured- thin-beds (FA3B). The lowermost unit (T3.1) (Fig. 8) coarsens upwards from coarse micro-rippled siltstone (palaeocurrents ~170°) (FA3A, >1 cm thick; Fig. 7E) to ripple laminated coarse sandstone (palaeocurrents throughout range from 010-335°, a 325° spread) (FA3B, ~4 cm thick; Figs. 7F, 8). The overlying unit (T3.2; ~2.5 m thick, Fig. 8) is characterised by multiple cm-deep scour surfaces that are orientated broadly W-E/NW-SE (090/270°-140/320°) and mantled with granules (Fig. 7F). The scour-fills comprise a matrix of medium-grained sandstone, with siltstone chips concentrated close to the scour surface but dispersed throughout. Scours are 3-5 cm in length (Fig. 7F), and exhibit relatively smooth bases, and a constant longitudinal maximum depth. Current ripple lamination throughout T3.2 give palaeocurrent measurements from 030-358° (a 328° spread). T3.3 (~1.5 m thick) comprises coarse grained sandstones (FA3B) with erosional bases, interbedded with planar laminated coarse siltstones (FA3A) with abundant current ripple lamination (palaeoflow 070-352°, a 282° spread) and grooves (palaeoflow 098/278°, 138/318°). The next 3 units (T3.4 – T3.6) are characterised by coarse planar laminated siltstone beds, interbedded with granule-rich sandstones (Fig. 8) that are current ripple laminated in T3.4 (palaeocurrent 040-110°, a 70° spread). Above this, sandstone beds thicken above deeper erosion surfaces, and contain abundant siltstone clasts distributed throughout. In summary, the scours and grooves are orientated approximately W-E to NW-SE, whilst the ripples show an almost 360° range of palaeocurrents (Fig. 4).

The base of Upper T3 is marked by a 20 cm thick granule-rich, very coarse-grained sandstone with an erosional base overlain by abundant siltstone clasts (Fig. 8). Six overlying beds (0.14 – 1.16 m thick) are normally graded from very coarse to fine sandstone or coarse siltstone with parallel lamination. This interval is overlain by a distinctive bed containing convex-upwards, low-angle lamination, inclined towards the main conduit (Fig. 7E), which resembles hummocky-cross stratification. Similar features have been documented by previous authors in turbidite systems, and in combination with palaeocurrent data are interpreted to form through deposition and reworking of reflected dilute flows (Mulder et al., 2009; Tinterri, 2011; Tinterri and Muzzi Magalhaes, 2011; Hofstra et al., 2018) forming a combined flow bedform. This is followed by six erosively-based normally graded and locally planar laminated sandstone beds, then a sandstone-dominated interval with multiple erosion surfaces mantled by siltstone clasts. This succession is cut by a surface overlain by extra- and intra-basinal small pebbles to large cobbles (up to 30 cm diameter) (Fig. 8). Overlying beds form fining-upwards packages of normally graded coarse to fine-grained sandstones, before the deposition of P4.

The elevated location of T1, T2 and T3 above the main conduit, the absence of physical bed-scale connections with axial deposits, the highly variable palaeocurrents (ripples with a full 360° range) and hummock-like bedforms indicating flow deflection/reflection/interaction, the distinctive thin-beds with multiple scours mantled with granules, and the absence of wedge-shaped stratigraphy or downlap, support the interpretation of these successions as terrace deposits (Hansen et al., 2015, 2017a, b; McArthur et al., 2019) with phases of sediment bypass, rather than internal levees (Kane and Hodgson, 2011) or channel margin deposits (Hubbard et al., 2014).

4.8 Regional correlation

The La Charca outcrop (~2 km up-dip from La Peña) is ~50 m thick (Figs. 2E-F), and exhibits a stepped basal surface that cuts into MTC 5, overlain by sandstone-prone deposits similar to FA2A, which are in turn overlain by laterally-thinning and/or amalgamated sandstone beds (<1-~10m thick) similar to FA2B (Fig. 2F). The stratigraphic continuity of MTD 5 and 6 and the absence of the sandbody in the 2 km between the outcrops of La Peña and La Charca (Figs. 2E-F), suggests a linear shape. Although the exact palaeoenvironmental relationship between the two outcrops is uncertain, the similar fill and geometry suggests some degree of connection. The stepped basal surface and overlying sandstone-prone succession similar to FA2A supports a channelised setting with basal lag deposits, with laterally discontinuous sandstones above interpreted as stacked individual channel bodies.

5 Discussion

5.1 Stratigraphic evolution

5.1.1 Formation of Surface 1 (S1)

The stepped geometry, and pebbly sandstones and conglomerates (FA2A) overlying S1 at the base of P1 and on the SW margin under P3 in the SSB, under the lowermost package of the NSB, and underlying T2 and T3 on elevated surfaces suggests that S1 deepened through multiple phases of erosion and sediment bypass. The SW expression of S1 in the SSB is characterised by onlap and localised erosion, indicating limited modification of S1 and MTD 5 during P1. This supports the formation of the composite S1 during an initial down-cutting phase dominated by sediment bypass (e.g. Hubbard et al., 2014; Hodgson et al., 2016), rather than reworking during aggradation. The ability of MTD 5 to support the formation of the remarkably steep gradients on S1 suggests a high yield strength and cohesion of the debrite (MTD 5), and contrasts with lower gradients recorded in submarine channels that incise into stratified substrates (e.g. Hansen et al., 2017a). Little information is available on the location of the NSB and SSB with respect to the large-scale morphology of the MTD body. The varying degrees of sandstone block disaggregation, thickness of the MTD and the lack of evidence of compressional thrust faulting suggests that the channels incise in the translational zone of the MTD body.

5.1.2 Channelised deposition (P1-P3)

P1 represents the first stage of fill within the SSB, and is characterised by coarse-grained amalgamated sandstones above the lowest part of the S1 surface (Fig. 9A). Overlying this, P2 is characterised by a wider grainsize range, fine-grained bed caps, and smaller-scale channelised bodies (Fig. 9B). During P2, flows eroded into the remobilised T1, and were able to deposit either side of the palaeohigh between the SSB and the NSB. The increase in fine grained material could either reflect a change in sediment source character, or a change in flow parameters resulting in reduced flow velocity and potential to bypass that affected grainsize sequestration along a system. The increase in finer material allowed formation and stabilisation of channels banks within the larger-scale conduit bounded by S1 (Peakall et al., 2007). The change in bed geometry may also reflect reduced confinement leading to lower local velocities and deposition and preservation of finer grainsizes, allowing elementary channels to form and migrate (Figs. 4, 9B). P3 is marked by tabular sandstone beds (Fig. 9C), with the greater bed thickness, coarser grain-size and level of amalgamation suggesting deposition from larger, higher energy flows, capable of bypassing finer-grained sediment down-dip (Kneller and Branney, 1995).

5.1.3 Downdip confinement

S2, an irregular and laterally-extensive erosion surface, cuts into P3 and T2 in both the SSB and the NSB, supporting an erosion- and bypass-dominated phase that resculpted both the SSB and NSB systems (Figs. 1, 4-5). This surface is overlain by a marked change to 6 m of interbedded FA4B (Figs. 5, 9D), which based on normally graded beds with fine grained caps, are interpreted as deposits of fully- or partially-confined flows (e.g. Sinclair and Tomasso, 2002). This abrupt change suggests the presence of downdip confinement of the channel system and formation of lobes. Complex palaeocurrents, ranging from 134-352° within this lower section further support the presence of down-dip confinement, with flow deflection and reflection off topography able to produce fully reversed measurements within a single deposit. The abrupt change from P3 to P4 is attributed to local changes within the system. Possible mechanisms include: 1) collapse of the unstable debrite wall after formation of S2 and plugging the conduit downdip; 2) the infilling of down-dip accommodation on top of the debrite through emplacement of an MTD; or 3) through continued deformation or (differential) compaction of the debrite impacting sediment transport pathways (e.g. Kneller et al., 2016; Zhao et al., 2019). The weak normal grading of L1 suggests that the scale of frontal flow confinement was limited, with fine-grained material transported further down-dip, and that the frontal confinement of lower P4 was related to emplacement of a minor MTD, possibly similar in size to MTD 6. Evidence for flow confinement decreases up stratigraphy, although complex palaeocurrent indicators indicate some topography remained.

5.1.4 Lobe progradation

P4 marks an abrupt change from channelised to lobe deposition. The extent of S2 to the NE of the NSB is unknown. However, the near-consistent bed thicknesses of L1-L4 suggest a lack of lateral compensational stacking, and therefore some confinement by S2 and that lobe development shows flow size was scalable to the size of S2. Examples of lobate deposits underlying a channel system in unconfined settings are well documented (e.g. Gardner et al., 2003; Macdonald et al., 2011; Hodgson et al., 2011, 2016). However, examples of lobes deposited within a channel are rarer. Lobes overlying individual channel complexes are associated with the 'spill' phase of channel development (Eschard et al., 2003; Gardner et al., 2003), and are unconfined. Lobes within the same confining surface as axial fill are undocumented, but semi-confined lobes have been documented in canyon settings in the South China Sea (Wu et al., 2018) and offshore Egypt (Morris et al., 2014).

Hybrid beds within channel confinement are rare, but have been documented in slope channel-fill of the Schiehallion Field (offshore the Shetland Islands), interpreted as a sign of system back-stepping or knickpoint migration (Haughton et al., 2009). Hybrid beds are more commonly associated with unconfined proximal (Fonnesu et al., 2015; Brooks et al., 2018), or lateral and frontal lobe fringe deposition (Haughton et al., 2003, 2009; Hodgson, 2009; Kane and Pontén, 2012; Kane et al., 2017; Spychala et al., 2017a, b, c). Several mechanisms may result in hybrid bed deposition within the channel system at La Peña, including: 1) system progradation where flow size remains the same, but as deposition was taking place in the upper portions of the channel cut, the conduit had sufficient width to allow 'unconfined' deposition from flows; 2) a reduction in flow size, resulting in underfit flows in relation to channel size forming 'unconfined' deposition (of hybrid beds); and 3) back-stepping of lobe complexes into the channel cut.

The thin-bedded sandstone-siltstone couplets (FA4B) in the lower section of P4 are interpreted as ponding of distal lobe fringe deposits, with increasing bed thickness and amalgamation of beds L1-L4, and decreasing volumes of fine-grained material suggesting progradation of a lobe complex. Erosional features in the lower portions of a lobe, such as the surface that truncates L1, are typically erosive products of larger flows (Fig. 4) which suggests sufficient space within S1 to allow ‘unconfined’ deposition at this point. Sand-rich hybrid beds similar to those seen in La Peña have been observed in areas proximal to the lobe axis (Fonnesu et al., 2015; Brooks et al., 2018). A similar configuration is supported by deposition of L5, which is characterised by amalgamated sandstone beds indicating a lobe axis.

5.1.5 Avulsion, lobe switching and back-stepping

The contact between Unit 2 and Unit 3 is a sharp change (Fig. 4, Log 9, 8 and 3, Fig. 6 top) from axial lobe to distal lobe fringe deposits, indicating a sudden change within the system. This corresponds with a change in palaeocurrent direction from the NW to the NE. The most likely mechanism for rapid abandonment of a lobe is upstream avulsion (Prélat et al., 2010; Macdonald et al., 2011). Therefore, Unit 3 represents distal lobe fringe deposition of a new lobe, or a phase of abandonment.

5.2 Terrace development

Multiple mechanisms can form terraced surfaces within submarine channel systems (Hansen et al., 2015), which then act as sites for subsequent deposition. The presence of FA2A on steps on S1 immediately below T2 and T3 suggest that these surfaces were once the location of much higher energy and coarser-grained flows that mainly bypassed sediment basinward, compared to the overlying deposits. This, coupled with S1 cutting down 10 m over a width of 18 m (a gradient of ~55°), and this elevation difference between T3 and the SSB (Fig. 4) suggests formation of the terraced surface was through bend cut-off by entrenchment (Hansen et al., 2015), with T3 deposited in the older elevated and abandoned channel cut. The spread in palaeocurrent data in lower T3 (Fig. 4) is indicative of flow deflection from frontal topography, with a large number of upstream flow indicators. Thus, plugging of the bend cut-off likely occurred through deposition at the ‘exit’ of the cut-off, possibly through reduced discharge and energy conditions within the abandoned channel that caused trapping of suspended sediment (Fisk, 1947; Constantine et al., 2010; Toonen et al., 2012). An intermediary high does not separate T1 and T2 from the main conduit, so the stepped surfaces these deposits are located on are likely entrenchment terrace surfaces (Babonneau et al., 2002, 2004; Hansen et al., 2015). The location of T1 adjacent to the NSB, and relationship with the base of P2, suggest T1 deposits were sourced from flows in the NSB, with flow deflection producing the dispersed palaeocurrent readings. Erosional terrace surfaces observed in the Indus and Benin-Major channel systems are interpreted to form during incision of the erosional fairway (Deptuck et al., 2003). Deposition on a terrace surface is governed by the thickness of a density-stratified turbidity current, and height of the terrace surface above the channel base (Hansen et al., 2015, 2017a, b). Consequently, assuming flow properties remain constant with time, increased height of terraces above the channel thalweg results in finer and thinner deposits (Babonneau et al., 2004, 2010). Thinning- and fining-upwards trends in external levees and terraces have been attributed to increased flow confinement (Hiscott et al., 1997; Normark et al., 1997; Kane and Hodgson 2011; Hansen et al., 2015).Thickening- and coarsening-upwards trends in levees have been interpreted to record system progradation of submarine fans (e.g. Mutti and Ricci Lucci, 1972; Hiscott, 1981; Mutti, 1984; Pickering et al., 1989) and as a function of lateral migration of a channel (Kane and Hodgson, 2011).

The thickest terrace succession (T3) exhibits two distinct styles of sedimentation separated by an abrupt change (Figs. 7D-G, 8). The lower portion (T3.1-T3.7) is finer-grained, and dominated by thin beds (Figs. 7D-E, 8), which form six thickening upwards packages (Fig. 8), suggesting formation by stripping of upper parts of flows in the channel axis of the SSB, and of either repeated aggradation of the channel, and/or cyclical external controls on flow magnitudes. The presence of scour surfaces mantled with coarse grains within the terrace deposits (Figs. 3H, 7F, 8) suggests that periodically there were more energetic, larger magnitude flows, or that periods of channel aggradation reduced the terrace height relative to the axis. Bed thickness, grainsize, and numbers of granule- and siltstone chip-rich intervals increase upwards in the upper T3 succession (Fig. 8). This change could record: a) higher aggradation of channel-axis deposits relative to terrace deposition, allowing increasingly coarse grainsizes and deposition of thicker beds, or b) increasing flow magnitude through time, possibly through system progradation, or c) some combination of the two. The overall pronounced coarsening-up succession of T3 suggests that the terrace deposits may largely reflect bed thalweg aggradation, rather than increasing flow magnitudes. Given that turbidity current velocity decreases exponentially with height, once above the height of the velocity maximum, then even large increases in flow magnitude are unlikely to be able to produce major scour surfaces and deposition of granules and siltstone chips (up to 1.5 cm in size) on highly elevated terraces (*sensu* Babonneau et al., 2004). Given the overall bed stacking with repeated minor coarsening-up cycles, the lower part of the terrace is most easily explained as recording successive phases of channel thalweg aggradation during the infill phase. If related to initial downcutting and formation of S1, then there would need to be six progressively larger phases of bed aggradation within the channel, followed by renewed downcutting. The abrupt change between the deposits of the lower and higher terrace suggests that there was a major phase of channel aggradation at this point, which may have been accompanied by increased flow size.

5.3 Relative Timing of the Southern Sandstone Body and Northern Sandstone Body fill

Faulting in the centre of the study area largely prevents tracing of stratigraphic surfaces between the SSB and the NSB. The relationship between P2 and T1 provides the oldest observational constraints available of the temporal evolution of SSB and NSB. The rotation, deformation, and incision of T1 (Fig. 7) suggests it was originally more extensive. The instability and remobilisation is likely related to a phase of erosion prior to deposition of P2. This indicates that the NSB was active prior to the deposition of P2, which is supported by the different depths of incision of the NSB and SSB. The NSB incision is ~15 m shallower than the SSB, and had they been contemporaneous, the SSB would have had a significant gradient advantage over the NSB, with the majority of flows transported through the SSB.

This may suggest that the NSB incised and filled prior to the incision by the SSB (Fig. 10Ai). The two channels may have formed from an updip avulsion, or by two separate channel systems (Fig. 10Aii). Channel avulsion can be triggered by a number of factors, including changes in slope gradient, channel aggradation and reduced channel relief, continued deformation of the debrite resulting in breaching of confinement, and channel plugging through MTD emplacement (Posamentier and Kolla, 2003; Kolla, 2007; Armitage et al., 2012; Ortiz Karpf et al., 2015). A number of these mechanisms can be discounted; there is no evidence for large scours or rapid deposition that is associated with a change in slope at this stratigraphic level. If channel plugging were responsible, evidence of confined or partially-confined flows (as seen in P4) would be expected, and no evidence of syn-sedimentary deformation (such as localised faulting, thinning or thickening of deposits away from the area of deformation, or deformation of deposits) is visible. The preferred mechanism in this scenario is a channel avulsion resulting from in-channel aggradation (Fig. 10Aii) that reduced channel relief, with the NSB representing the original channel, and the SSB the post-avulsion channel (Figs. 10Aiii-iv).

Alternatively, it may be the case that the NSB and SSB were coeval. Subtle variations in channel morphology and thalweg gradient can influence flow velocity, and thus the erosion-deposition threshold (Kneller, 1995; Stevenson et al., 2015). A steeper gradient in the SSB would result in more sediment bypass through this channel, whilst deposition occurred in the NSB (Fig. 10Bi). When available accommodation within the NSB was filled, all flows would be diverted down the SSB (Fig. 10Bii), which begins to aggrade (Fig. 10Biii). It is also possible that the NSB and SSB are related to an upstream knickpoint migration and splitting upon reaching a more resistant lithology. Buried megaclasts could have formed lithological contrasts, and influenced surface sediment routing long after burial (Alves and Cartwright, 2010; Ward et al. 2018). A further possibility is that NSB and SSB could represent two channel systems that developed above the MTD 5 debrite independently, but in close proximity, as seen beyond the shelf-edge delta in the Fuji-Einstein system (Gulf of Mexico, Sylvester et al., 2012). The transition from erosion and bypass to aggradation within the NSB suggests a waning sediment supply, with depositional flows having limited ability to erode and form new conduits, meaning channel development was likely coeval.

5.4 Source-to-sink implications

A striking aspect of the exhumed parts of the deep-marine stratigraphy in the study area is the scarcity of channel-fills despite the profusion of large MTDs (Valdez Buso et al., 2019). Furthermore, channel-fills are not recorded in other exposed parts of the Valle Fértil sub-basin-fill (cf. Fernandez-Seveso and Tankard, 1995). Turbidite lobes are widely identified (Fallgatter et al., 2019), which suggests the presence of lower order distributary channel systems. The bounding turbidite stratigraphy below and above the studied succession are interpreted as prograding turbiditic wedges, similar to the succession observed at Cerro Bola from the maximum flooding zone of Cycle 3 (cf. Fallgater et al, 2017, Valdez Buso et al., 2020).

The La Peña channel-fills documented here are an anomaly in this basin-fill. Therefore, we link the development of the channels to the perturbation of the sedimentary system by emplacement of the MTD 5 debris flow. Furthermore, the abrupt influx of coarse sands suggests modification of the updip drainage system after emplacement of the debris flow such that coarser material became a source. Emplacement of a large submarine landslide forces not only changes in sediment sources and dispersal patterns, but also grain size segregation.

This has implications for subsurface appraisal on hydrocarbon and carbon reservoirs (e.g. Steventon et al., 2021), as the failure that generated MTD 5 created the transient conditions that segregated sand and mud more effectively, making the sand-prone channel-fills potential hydrocarbon traps, that otherwise would never have developed. In other words, without MTD 5, the system would likely have maintained a poor grain-size separation. This case study demonstrates the dramatic changes large submarine landslides impose on pre-existing drainage and sediment dispersal patterns.

6 Conclusions

Here we present the first study of two exceptionally well-exposed erosional channel systems (the NSB and SSB) that incised into a thick megaclast-bearing debrite. We also document the formation and flow-scale evolution of a seismic-scale outcrop, using sedimentological analysis, geological mapping and photogrammetric modelling. We demonstrate the ability of flows to progressively incise >75 m into an underlying MTD, a debrite, with remarkably steep margins (up to 70°). The evolution from erosion- and sediment bypass-dominated to deposition-dominated is marked by aggradational stacking of sand-rich channel-fill, exhibiting a high degree of homogeneity. Above this, stepped changes in confinement coincided with a change in intrachannel architecture to laterally-migrating channel bodies, follows by tabular, highly-aggradational fill. Furthermore, we examine the sedimentological and stratigraphic evolution of two types of depositional terrace: an entrenchment terrace, and the first outcrop example of a terrace deposit situated in a bend cut-off. We show progradation of a lobe complex within the larger channel erosion surface, characterised by a lack of compensational stacking and increasingly thick deposits of proximal lobe hybrid bed deposits. The scarcity of channel-fills in the rest of the exhumed deep-water stratigraphy, and the abrupt influx of coarse sand, indicates a clear link between perturbation of the sedimentary system by emplacement of MTD 5 and the inception and evolution of the overlying channels. This study shows that emplacement of a large submarine landslide can abruptly change sediment sources and dispersal patterns, and facilitates effective segregation of grain sizes in deep-marine environments.

7 References

Allen, J.R.L., 1984. Parallel lamination developed from upper-stage plane beds: A model based on the larger coherent structures of the turbulent boundary layer. Sedimentary Geology, 39, 227–242. https:// doi .org /10 .1016 /0037 -0738 (84)90052 -6.

Allmendinger, R., Figueroa, D., Snyder, D., Beer, J., Mpodozis, C. Isacks, B., 1990. Foreland shortening and crustal balancing in the Andes at 30°S latitude. Tectonics, 9, 789-809.

Alves, T.M., Cartwright, J.A., 2010. The effect of mass-transport deposits on the younger slope morphology, offshore Brazil. Marine and Petroleum Geology 27, 2027-2036.

Armitage, D.A., McHargue, T., Fildani, A., Graham, S.A., 2012. Postavulsion channel evolution: Niger Delta continental slope. AAPG Bulletin, 96, 823–843.

Astini, R.A., Benedetto, J.L., Vaccari, N.E., 1995. The Early Paleozoic evolution of the Argentine Precordillera as a Laurentian rifted, drifted and collided terrane: a geo- dynamic model. GSA Bulletin, 107, 253–273.

Bart, P.J., De Batist, M., Jokat, W., 1999. Interglacial collapse of Crary trough-mouth fan, Weddell Sea, Antarctica: implications for Antarctic glacial history. Journal of Sedimentary Research, 69, 1276–1289.

Babonneau, N., Savoye, B., Cremer, M., Klein, B., 2002. Morphology and architecture of the present canyon and channel system of the Zaire deep-sea fan. Marine and Petroleum Geology, 19, 445–467.

Babonneau, N., Savoye, B., Cremer, M., Bez, M., 2004. Multiple terraces within the deep incised Zaire Valley (ZaïAngo Project): are they confined levees? In: Lomas, S. A., Joseph, P. (Eds.), Confined Turbidite Systems. Geological Society, London, Special Publications 222, 91-114.

Babonneau, N., Savoye, B., Cremer, M., Bez, M., 2010. Sedimentary architecture in meanders of a submarine channel: detailed study of the present Congo turbidite channel (ZAIANGO project). Journal of Sedimentary Research, 80, 852–866.

Best, J., Bridge, J., 1992. The morphology and dynamics of low amplitude bedwaves upon upper stage plane beds and the preservation of planar laminae. Sedimentology, 39, 737-752.

Beaubouef, R.T., Savoye, B., Cremer, M., Bez, M., 2004. Deep-water leveed channel complexes of the Cerro Toro Formation, Upper Cretaceous, southern Chile. AAPG Bulletin, 88, 1471–1500.

Bouma, A., 1962. Sedimentology of some Flysch Deposits: A Graphic Approach to Facies Interpretation. Elsevier, Amsterdam/New York, 168 pp.

Brooks, H.L., Hodgson, D.M., Brunt, R.L., Peakall, J., Hofstra, M., Flint, S.S., 2018. Deep-water channel-lobe transition zone dynamics: processes and depositional architecture, an example from the Karoo Basin, South Africa. GSA Bulletin, 130, 1723–1746.

Bull, S., Browne, G.H., Arnot, M.J., Strachan, L.J., 2020. Influence of Mass Transport Deposit (MTD) surface topography on deep-water deposition: an example from a predominantly fine-grained continental margin, New Zealand. In: Georgiopoulou, A., Amy, L.A., Benetti, S., Chaytor, J.D., Clare, M.A., Gamboa, D., Haughton, P.D.W., Moernaut, J., Mountjoy, J.J., (Eds.), Subaqueous Mass Movements and their Consequences: Advances in Process Understanding, Monitoring and Hazard Assessments. Geological Society, London, Special Publications, 500, 147-171.

Constantine, J.A., Dunne, T., Piégay, H., Kondolf, G.M., 2010. Controls on the alluviation of oxbow lakes by bed-material load along the Sacramento River, California. Sedimentology 57, 389–407.

Deptuck, M.E., Steffens, G.S., Barton, M., Pirmez, C., 2003. Architecture and evolution of upper fan channel belts on the Niger Delta slope and in the Arabian Sea. Marine and Petroleum Geology, 20, 649-676.

Dott, J. 1963. Dynamics of Subaqueous Gravity Depositional Processes. AAPG Bulletin 47(1), 104–128.

Elverhøi, A., Hooke, R.L.B., Solheim, A., 1998. Late Cenozoic erosion and sediment yield from the Svalbard–Barents Sea region: implications for understanding erosion of glacierized basins. Quaternary Science Reviews, 17, 209–241.

Eyles, C.H., Eyles, N., Miall, A.D., 1985. Models of glaciomarine deposition and their applications to ancient glacial sequences. Palaeogeography, Paleoclimatology and Palaeoecology, 51, 15–84.

Fallgatter, C., Kneller, B., Paim, P.S., Milana, J.P., 2017. Transformation, partitioning and flow–deposit interactions during the run-out of megaflows. Sedimentology, 64, 359-387.

Fallgatter, C., Valdez Buso, V., Paim. P.S.G., Milana, J.P., 2019. Stratigraphy and depositional architecture of lobe complexes across a range of confinements: Examples from the Late Paleozoic Paganzo Basin, Argentina, Marine and Petroleum Geology, 110, 254-274. DOI: 10.1016/j.marpetgeo.2019.07.020.

Fernández-Seveso, F., Tankard, A.J., 1995. Tectonics and stratigraphy of the late Paleozoic Paganzo Basin of Western Argentina and its regional implications, in: Tankard, A.J., Suarez, S., Welsink, H.J., (Eds.), Petroleum basins of South America. AAPG Memoirs 62, 285–301.

Fisk, H.N., 1947. Fine grained alluvial deposits and their effect on Mississippi River activity, Volumes 1 & 2. Mississippi River Commission: Vicksburg, MS.

Fonnesu, M., Haughton, P., Felletti, F., McCaffrey, W., 2015. Short length-scale variability of hybrid event beds and its applied significance. Marine and Petroleum Geology, 67, 583–603.

Gardner, M.H., Borer, J.M., Melik, J.J., Mavilla, N., Dechesne, M., Wagerle, R.D., 2003. Stratigraphic process-response model for submarine channels and related features from studies of Permian Brushy Canyon outcrops, West Texas. Marine and Petroleum Geology, 20, 757–788.

Hansen, L.A.S., Callow, R.H.T., Kane, I.A., Gamberi, F., Rovere, M., Cronin, B.T., Kneller, B.C., 2015. Genesis and character of thin-bedded turbidites associated with submarine channels. Marine and Petroleum Geology 67, 852–879.

Hansen, L.A.S., Janocko, M., Kane, I., Kneller, B., 2017a. Submarine channel evolution, terrace development, and preservation of intra-channel thin-bedded turbidites: Mahin and Avon channels, offshore Nigeria. Marine Geology, 383, 146–167.

Hansen, L.A.S., Callow, R., Kane, I.A., Kneller, B.C., 2017b. Differentiating submarine channel related thin-bedded turbidite facies: Outcrop example from the Rosario Formation, Mexico. Sedimentary Geology, 358, 19–34.

Hiscott, R.N., 1981. Deep sea fan deposits in the Macigno Formation (Middle-Upper Oligocene) of the Gordana Valley, Northern Apennines, Italy: Discussion. Journal of Sedimentary Petrology, 51, 1015-1021.

Hodgson, D.M., 2009. Distribution and origin of hybrid beds in sand-rich submarine fans of the Tanqua depocentre, Karoo Basin, South Africa. Marine and Petroleum Geology, 26, 1940–1956. https://doi.org/10.1016/j.marpetgeo.2009.02.011.

Hodgson, D.M., Haughton, P.D.W., 2004. Impact of syn-depositional faulting on gravity current behaviour and deep-water stratigraphy: Tabernas–Sorbas Basin, SE Spain. In: Lomas, S., Joseph, P. (Eds.), Confined Turbidites Systems. Geological Society, London, Special Publications 222, 135–158.

Hodgson, D.M., Di Celma, C.N., Brunt, R.L., Flint, S.S., 2011. Submarine slope degradation and aggradation and the stratigraphic evolution of channel–levee systems. Journal of the Geological Society of London, 168, 625–628.

Hodgson, D.M., Kane, I.A., Flint, S.S., Brunt, R.L., Ortiz-Karpf, A., 2016. Time-transgressive confinement on the slope and the progradation of basin-floor fans: implications for the sequence stratigraphy of deep-water deposits. Journal of Sedimentary Research, 86, 73–86. https://doi.org/10.2110/jsr.2016.3.

Hofstra, M., Peakall, J., Hodgson, D.M., Stevenson, C.J., 2018. Architecture and morphodynamics of subcritical sediment waves in an ancient channel–lobe transition zone. Sedimentology, 65, 2239-2367. https://doi.org/10.1111/sed.12468.

Hubbard, S.M., Covault, J.A., Fildani, A., Romans, B.W., 2014. Sediment transfer and deposition in slope channels: deciphering the record of enigmatic deep-sea processes from outcrop. GSA Bulletin, 126, 857–871.

Jegou, I., Savoye, B., Pirmez, C., Droz, L., 2008. Channel-mouth lobe complex of the recent Amazon Fan; the missing piece. Marine Geology, 252, 62–77.

Kane, I.A., Hodgson, D.M., 2011. Sedimentological criteria to differentiate submarine channel levee sub-environments: exhumed examples from the Rosario Fm. (Upper Cretaceous) of Baja California, Mexico, and the Fort Brown Fm. (Permian), Karoo Basin, S. Africa. Maine and Petroleum Geology, 28, 807–823.

Kane, I.A., Pontén, A.S.M., 2012. Submarine transitional flow deposits in the Paleogene Gulf of Mexico. Geology, 40, 1119–1122. https://doi.org/10.1130/G33410.1.

Kane, I.A., Kneller, B.C., Dykstra, M., Kassem, A., McCaffrey, W., 2007. Anatomy of a submarine channel–levee: an example from Upper Cretaceous slope sediments, Rosario Formation, Baja California, Mexico. Marine and Petroleum Geology, 24, 540–563.

Kneller, B., 1995. Beyond the turbidite paradigm, physical models for deposition of turbidites and their implications for reservoir prediction. In: Hartley, A.J., Prosser, D.J. (Eds.), Characterization of Deep-Marine Clastic Systems. Geological Society, London, Special Publications 94, 31-49.

Kneller, B.C., Branney, M.J., 1995. Sustained high-density turbidity currents and the deposition of thick massive sands. Sedimentology, 42, 607-616.

Kneller, B., McCaffrey, W., 1999. Depositional effects of flow nonuniformity and stratification within turbidity currents approaching a bounding slope: deflection, reflection, and facies variation. Journal of Sedimentary Research, 69, 980-991.

Kneller, B. C., Edwards, D., McCaffrey, W., Moore, R., 1991. Oblique reflection of turbidity currents. Geology, 19, 250–252.

Kneller, B., Dykstra, M., Fairweather, L., Milana, J.P., 2016. Mass-transport and slope accommodation: implications for turbidite sandstone reservoirs. AAPG Bulletin, 100, 213–235.

Kolla, V., 2007. A review of sinuous channel avulsion patterns in some major deep- sea fans and factors controlling them. Marine and Petroleum Geology, 24, 450-469. http:// dx.doi.org/10.1016/j.marpetgeo.2007.01.004

Limarino, C.O., Cesari, S.N., Net, L.I., Marenssi, S.A., Gutierrez, R.P., Tripaldi, A., 2002. The Upper Carboniferous postglacial transgression in the Paganzo and Rio Blanco basins (northwestern Argentina): Facies and stratigraphic significance. Journal of South American Earth Sciences, 15(4), 445–460. doi:10.1016/ S0895-9811(02)00048-2

Limarino, C.O., Tripaldi, A., Marenssi, S., Fauque, L., 2006. Tectonic, sea level and climatic controls on Late Palaeozoic sedimentation in the western basins of Argentina. Journal South American Earth Sciences, 22, 205–226.

Limarino, C.O., Césari, S.N., Spalletti, L.A., Taboada, A.C., Isbell, J.L., Geuna, S., Gulbranson, E.L., 2014. A paleoclimatic review of southern South America during the late Paleozoic: A record from icehouse to extreme greenhouse conditions. Gondwana Research, 25, 1396-1421, DOI: 10.1016/j.gr.2012.12.022.

López-Gamundí, O., Martínez, M., 2000. Evidence of glacial abrasion in the Calingasta Uspallata and western Paganzo basins, mid-Carboniferous of western Argentina. Palaeogeography, Palaeoclimatology, Palaeoecology, 159, 145–165.

Lowe, D.R., 1982. Sediment gravity flows: II. Depositional models with special reference to the deposits of high-density turbidity currents. Journal of Sedimentary Petrology, 52, 279–297.

Lowe, D.R., 1988. Suspended-load fallout rate as an independent variable in the analysis of current structures. Sedimentology, 35, 765-776.

MacDonald, H.A., Peakall, J., Wignall, P.B., Best, J., 2011. Sedimentation in deep-sea lobe-elements: implications for the origin of thickening-upward sequences. Journal of the Geological Society, 168, 319–331.

Mantz, P.A., 1978. Bedforms produced by fine, cohesionless, granular and flakey sediments under subcritical water flows. Sedimentology, 25, 83-103.

McArthur, A., Kane, I.A., Bozetti, G., Hansen, L.A.S., Kneller, B.C., 2019. Supercritical flows overspilling from bypass - dominated submarine channels and the development of overbank bedforms. The Depositional Record, 6, 21-40.

Milana, J.P., 1992. Estratigrafía secuencial, cortejos sedimentarios y su relación con la evolución geotectónica de la cuenca Paleozoica inferior de la Precordillera. IV Reunión Arg. Sedimentología, La Plata, actas, 2, 199-206.

Milana, J.P., Alcober, O., 1994. Modelo tectosedimentario de la cuenca triásica de Ischigualasto (San Juan, Argentina). Revista Asociación Geológica Argentina, 49, 217-235.

Milana, J.P., Di Pasquo, M.M., 2019, New chronostratigraphy for a lower to upper Carboniferous strike-slip basin of W-Precordillera (Argentina): Paleogeographic, tectonic and glacial importance: Journal of South American Earth Science, 96, 102383. https://doi.org/10.1016/j.jsames.2019.102383

Milana, J.P., Kneller, B., Dykstra, M., 2010. Mass-transport Deposits and Turbidites, Syn- to-Post-Glacial Carboniferous Basins of Western Argentina. ISC 2010 Field Guide, 01–88.

Milliman, J.D., Meade, R.H., 1983. World-wide delivery of river sediment to the oceans. The Journal of Geology, 91, 1–21.

Morris, E.A., Hodgson, D.M., Flint, S.S., Brunt, R.L., Butterworth P.J., Verhaeghe, J., 2014. Sedimentology, Stratigraphic Architecture, and Depositional Context of Submarine Frontal-Lobe Complexes. Journal of Sedimentary Research, 84, 763-780.

Moscardelli, L., Wood, L., Mann, P., 2006. Mass-transport complexes and associated processes in the offshore area of Trinidad and Venezuela. AAPG Bulletin, 90, 1059–1088.

Mpodozis, C., Ramos, V.A., 1989. The Andes of Chile and Argentina. In: G. E Ericksen, M. T. Cañas Pinochet, and J. A. Reinemud, (Eds.), Geology of the Andes and its relations to hydrocarbon and mineral resources. Circum-Pacific Council for Energy and Mineral Resources, Earth Science Series, 11, 59–90.

Mulder, T., Alexander, J., 2001. The physical character of subaqueous sedimentary density flows and their deposits. Sedimentology, 48, 269–299.

Mulder, T., Zaragosi, S., Razin, P., Grelaud, C., Lanfumy, V., Bavoil, F., 2009. A new conceptual model for the deposition process of homogenite: application to a Cretaceous megaturbidite of the western Pyrenees (Basque region, SW France). Sedimentary Geology, 222, 263–273.

Mutti, E., 1984. The Hecho Eocene submarine fan system, south-central Pyrenees, Spain. Geo Marine Letters, 3, 199–202. https://doi.org/10.1007/BF02462468.

Mutti, E., 1992. Turbidite Sandstones. Agip -Instituto di Geologia, Università di Parma, Italy, 275p.

Mutti, E., Normark, W.R., 1987. Comparing examples of modern and ancient turbidite systems, problems and concepts. In: Leggett, J.K., Zuffa, G.G., (Eds.), Marine Clastic Sedimentology, Concepts and Case Studies. London. Graham and Trotman, London, 1-37.

Nardin, T.R., Hein, F.J., Gorsline, D.S., Edwards, B.D., 1979. A review of mass movement processes, sediment and acoustic characteristics, and contrasts in slope and base-of-slope systems versus canyon-fan-basin floor systems. In: Doyle, L.J., Pilkey, O.H. (Eds.), Geology of Continental Slopes. SEPM Society for Sedimentary Geology, Special Publication 27, 61-73.

Nelson, C.H., Escutia, C., Damuth, J.E., Twichell, D.C., 2011. Interplay of mass-transport and turbidite-system deposits in different active tectonic and passive continental margin settings: external and local controlling factors. In: Shipp, R.C., Weimer, P., Posamentier, H.W. (Eds.), Mass-transport Deposits in Deepwater Settings. SEPM Society for Sedimentary Geology, 39–66.

Ortiz-Karpf, A., Hodgson, D.M., McCaffrey, W.D., 2015. The role of mass-transport complexes in controlling channel avulsion and the subsequent sediment dispersal patterns on an active margin: The Magdalena Fan, offshore Colombia. Marine and Petroleum Geology, 64, 58–75.

Pazos, P.J., 2002. The Late Carboniferous glacial to postglacial transition; facies and sequence stratigraphy, western Paganzo Basin, Argentina. Gondwana Research, 5, 467–487.

Peakall, J., Ashworth, P.J., Best, J.L., 2007, Meander bend evolution, alluvial architecture, and the role of cohesion in sinuous river channels: a flume study. *Journal of Sedimentary Research*, 77, 197-212.

Peakall, J., Best, J., Baas, J.H., Hodgson, D.M., Clare, M.A., Talling, P.J., Dorrell, R.M., Lee, D.R., 2020. An integrated process-based model of flutes and tool marks in deep- water environments: Implications for palaeohydraulics, the Bouma sequence and hybrid event beds. Sedimentology, 67, 1601–1666.

Pett, J.W., Walker, R.G., 1971. Relationship of flute cast morphology to internal sedimentary structures in turbidites. Journal of Sedimentary Petrology, 41, 114–128.

Pickering, K.T., Hiscott, R.N., Hein, F.J., 1989. Deep-Marine Environments. Unwin Hyman, London, 416 pp.

Piper, D.J.W., Normark, W.R., 1983. Turbidite depositional patterns and flow characteristics, Navy submarine fan, California Borderland. Sedimentology, 30, 681–694.

Piper, D.J.W., Pirmez, C., Manley, P.L., Long, D., Flood, R.D., Normark, W.R., Showers, W., 1997. Mass transport deposits of the Amazon Fan. In: Flood, R.D., Piper, D.J., Klaus, A., Peterson, L.C. (Eds.), Proceedings or the Ocean Drilling Program, Scientific Results, Amazon Fan 155. Ocean Drilling Program, College Station, Texas, 109-146.

Pirmez, C., Flood, C., 1995. Morphology and structure of Amazon channel. In: Flood, R.D., Piper, D.J.W., Klaus, A., Peterson, L.C., (Eds.), Proceedings of the Ocean Drilling Program, Initial Reports 155. Ocean Drilling Program, College Station, Texas, 23-45.

Prélat, A., Hodgson, D.M., Flint, S.S., 2009. Evolution, architecture and hierarchy of distributary deep-water deposits: a high-resolution outcrop investigation from the Permian Karoo Basin, South Africa. Sedimentology, 56, 2132–2154.

Prélat, A., Covault, J.A., Hodgson, D.M., Fildani, A., Flint, S.S., 2010. Intrinsic controls on the range of volumes, morphologies, and dimensions of submarine lobes. Sedimentary Geology, 232, 66-76. http://dx.doi.org/10.1016/j.sedgeo.2010.09.010.

Posamentier, H.W., 2003. Depositional elements associated with a basin- floor channel–levee system: case study from the Gulf of Mexico. Marine and Petroleum Geology, 20, 667–690.

Qin, Y.P., Alves, T.M., Constantine, J., Gamboa, D., 2017. The role of mass wasting in the progressive development of submarine channels (Espirito Santo Basin, SE Brazil). Journal of Sedimentary Research, 87, 500–516.

Ramos, V.A., 1988. The tectonics of central Andes; 30°–33°S latitude. In: Clark, S., Burchfield, D., (Eds.), Processes in continental lithosphere deformation. Geological Society of America, Special Paper, 218, 31–54.

Ramos, V. A., Jordan, T.E., Allmendinger, R.W., Mpodozis, C., Kay, S.M., Cortes, J.M., Palma, M.A., 1986. Paleozoic terranes of the central Argentine–Chilean Andes. Tectonics, 5, 855–880.

Rees, A.I., 1966. Some flume experiments with a fine silt. Sedimentology, 6, 209-240.

Salfity, J.A., Gorustovich, S.A., 1983. Paleogeografía de la Cuenca de Paganzo (Paleozoico Superior). Revista Asociación Geológica Argentina 38, 437–453.

Sinclair, H.D., Tomasso, M., 2002. Depositional evolution of confined turbidite basins. Journal of Sedimentary Research, 72, 451-456.

Sobiesiak, M., Kneller, B., Alsop, I.G., Milana, J.P., 2016. Internal deformation and kinematic indicators within a tripartite mass transport deposit, NW Argentina. Sedimentary Geology, 344, 364-381.

Sobiesiak, M.S., Alsop, G.I., Kneller, B., Milana, J.P., 2017. Sub-seismic scale folding and thrusting within an exposed mass transport deposit: A case study from NW Argentina. Journal of Structural Geology, 96, 176-191.

Southard, J.B., 1991. Experimental determination of bed-form stability. Annual Review of Earth and Planetary Sciences, 19, 423-455.

Spychala, Y.T., Hodgson, D.M., Prélat, A., Kane, I.A., Flint, S.S., Mountney, N.P., 2017a. Frontal and lateral submarine lobe fringes: comparing facies, architecture and flow processes. Journal of Sedimentary Research, 87, 1–21.

Spychala, Y.T., Hodgson, D.M., Stevenson, C.J., 2017b. Aggradational lobe fringes: the influence of subtle intrabasinal seabed topography on sediment gravity flow processes and lobe stacking patterns. Sedimentology, 64, 582–608. https://doi.org/10. 1111/sed.12315.

Spychala, Y.T., Hodgson, D.M., Lee, D.R., 2017c. Autogenic controls on hybrid bed distribution in submarine lobe complexes. Marine and Petroleum Geology, 88, 1078-1093.

Stevenson, C.J., Jackson, C.A.-L., Hodgson, D.M., Hubbard, S.M., Eggenhuisen, J.T., 2015. Deep-water sediment bypass. Journal of Sedimentary Research 85, 1058-1081.

Steventon, M.J., Jackson, C.A-L., Johnson, H.D., Hodgson, D.M., Kelly, S., Omma, J., Gopon, C., Stevenson, C., Fitch, P., 2021. Evolution of a sand-rich submarine channel-lobe system and impact of mass-transport and transitional flow deposits on reservoir heterogeneity: Magnus Field, northern North Sea. Petroleum Geoscience, 27, petgeo2020-095. https://doi.org/10.1144/petgeo2020-095.

Stow, D.A.V., Johansson, M., 2002. Deep-water massive sands: nature, origin and hydrocarbon implications. Marine and Petroleum Geology 17, 145–174.

Sumner, E.J., Amy, L., Talling, P.J., 2008. Deposit structure and processes of sand deposition from a decelerating sediment suspension. Journal of Sedimentary Research 78, 529–547.

Sylvester, Z., Deptuck, M.E., Prather, B., Pirmez, C., O'Byrne, C., 2012. Seismic stratigraphy of a shelf-edge delta and linked submarine channels in the NE Gulf of Mexico. In: Prather, B., Deptuck, M., Mohrig, B., Van Hoor, B., Wynn, R.B., (Eds.), Application of the principles of seismic geomorphology to continental slope and base-of-slope systems: case studies from seafloor and near-seafloor analogues. SEPM Society for Sedimentary Geology, Special Publication 99, 31–59.

Talling, P.J., Amy, L.A., Wynn, R.B., Peakall, J., Robinson, M., 2004. Beds comprising debrite sandwiched within co-genetic turbidite: origin and widespread occurrence in distal depositional environments. *Sedimentology*, *51*, 163-194.

Talling, P.J., Masson, D.G., Sumner, E.J., Malgesini, G., 2012. Subaqueous sediment density flows: depositional processes and deposit types. Sedimentology 59, 1937-2003.

Thompson, R., Mitchell, J.G., 1972. Palaeomagnetic and radiometric evidence for the age of the lower boundary of the Kiaman magnetic interval in South America. Geophysical Journal International, 27, 207-214.

Tinterri, R., 2011. Combined flow sedimentary structures and the genetic link between sigmoidal and hummocky cross-stratification. GeoActa (Bologna) 10,1–43.

Tinterri, R., Muzzi Magalhaes, P., 2011. Syn-sedimentary structural control on foredeep turbidites: an example from Miocene Marnoso-arenacea Formation, Northern Apennines, Italy. Marine and Petroleum Geology 28, 629–657.

Toonen, W.H.J., Kleinhans, M.G., Cohen, K.M., 2012. Sedimentary architecture of abandoned channel fills. Earth Surface Processes and Lanforms 37, 459–472.

Valdez Buso, V., Milana, J. P., Sobiesiak, M. S., Kneller, B., 2019. The Carboniferous MTD Complex at La Peña Canyon, Paganzo Basin (San Juan, Argentina). In: Otaga, K., Festa, A., Pini, G.A., (Eds.), Submarine Landslides: Subaqueous Mass Transport Deposits from Outcrops to Seismic Profiles. Geophysical Monograph Series 246, 105-115.

Valdez Buso, V., Milana, J.P., di Pasquo, M., Paim, P.S.G., Philipp, R.P., Aquino, C.D., Cagliari, J., Junior, F.C., Kneller, B., 2020. Timing of the Late Palaeozoic glaciation in western Gondwana: New ages and correlations from Paganzo and Paraná basins. Palaeogeography, Palaeoclimatology, Palaeoecology, 544, 109624.

Valdez Buso, V., Milana, J.P., di Pasquo, M., Aburto, J.E., 2021. The glacial paleovalley of Vichigasta: Paleogeomorphological and sedimentological evidence for a large continental ice-sheet for the mid-Carboniferous over central Argentina. Journal of South American Earth Sciences, 106, 103066.

Ward, I.P.N., Alves, M.T., Blenkinsop, G.T., 2018. Submarine sediment routing over a blocky mass-transport deposit in the Espirito Santo Basin, SE Brazil. Basin Research 30, 816–834.

Winn, R.D., Dott, R.H., 1977. Large-scale traction structures in deep-water fan-channel conglomerates in southern Chile. Geology 5, 41–44.

Zavala, C., Pan, S., 2018. Hyperpycnal flows and hyperpycnites: Origin and distinctive characteristics. Lithological Reservoirs 30, 1-27.

Zhao, X.M., Qi, K., Patacci, M., Tan, C.P., Xie, T., 2019. Submarine channel network evolution above an extensive mass-transport complex: A 3D seismic case study from the Niger delta continental slope. Marine and Petroleum Geology 104, 231–248.

Figure captions:

Figure 1. (A) Image of the Paganzo Basin, with inset showing location within South America. Study area is located within black box. (B) Enlargement of the study area, showing the location of the La Peña outcrops, where fieldwork was undertaken, and the La Charca outcrop, described using outcrop modelling and photographs. (C) Stratigraphic column (adapted from Valdez Buso et al., 2019), showing the regional stratigraphy, and La Peña stratigraphy in detail from data herein. (D) Geological map of La Peña study area, showing the deposits studied in this paper.

Figure 2. (A) Aerial photograph of the field area (used in Fig. 1B) showing the relative location of outcrops, with arrows pointing to point of view of photographs in A, B, D and E. Outcrop images from (B) the Southern Channel of La Peña outcrop. (C) The Northern Channel of the La Peña outcrop. (D) Contact between channel sand and MTD, in the Southern Channel of La Peña outcrop, seen from the fault plane shown in Fig. 2A. (E) Image of the up-dip La Charca outcrop (see Fig. 2C), with line drawing overlay showing interpreted architecture. (F) Close-up of La Charca outcrop, showing internal channel bodies and clast-rich basal layers. T1, T2 and T3 are interpreted terrace deposits.

Figure 3. Representative facies photographs from outcrops at La Peña. (A) Lower sand block-rich, and mid sections of MTD 5, showing decreasing concentration of sand blocks up section. MTD basal contact with underlying stratigraphy is also seen. (B) Deformed contact between FA1B and overlying sandstone. (C) Sand-rich imbricate thrust sheets of MTD 6. (D) Basal conglomerate layer from the Southern Channel. (E) Massive, amalgamated coarse-grained turbidite deposition. (F) Fine-grained sand bed cap of channelised bed geometries. (G) Fissile, thin-bedded terrace deposits (H) Scoured and gravel-rich thin-bedded terrace deposits (I) Repeated sand-mud couplets (J) Sharp contact between sand and underlying mud. (K) Massive sandstone with overlying linked debrite. (L) Massive, planar and ripple laminated mica-rich sandstone.

Figure 4. Correlation panel for SSB, and associated palaeocurrent data. Correlation panel is split into stratigraphic packages based on lithology and bed geometry. Additional palaeocurrent data is from an uplifted section of the SSB base. Outcrop line drawing shows location of sedimentary logs, and bed geometries within the Southern Channel. The 77 m between the channel axis and the terraces are shortened to fit these features onto the line drawing. The inset figure in the lower left is from a UAV photograph of the 3D outcrop, so perspective is different. Furthermore, some beds are exposed at an angle and do not show true vertical thickness. The correlation panel is based on true thicknesses.

Figure 5. Outcrop image and sedimentary logs showing architecture and lithology of Package 4. (A) Panorama showing the western section of Package 4 within the channel axis. Lobes 1-4 are visible, as is the base of lobe 5. (B) Sedimentary logs showing the lateral change in lithology between the part of Package 4 containing L1, and the part where L1 has been truncated by a small channel, both of which are underlain by the first incidence of ponded sand-mud couplets. Top of log shows L2. (C) Log through the middle of Package 4, showing L3 and overlying hybrid bed deposition. (D) Sedimentary log through the upper section of Package, showing L4. D* Upper package of hybrid beds and L5 are not visible from this position as they are above the line of sight from this angle, but are included in Fig. 5D.

Figure 6. Correlation panel for the NSB, and associated palaeocurrent data. P4 and overlying stratigraphy is present in the NSB, but underlying stratigraphy cannot be correlated with the SSB. Log location shown in Fig. 1D.

Figure 7. Examples of terraces in the La Peña section. (A) Outcrop of T1, showing slip surface, and over-spilling channel sand eroding the terrace deposition. (B) Closer image showing the erosion of channel sand, and the predominantly thin-bedded nature of the terrace. (C) Medium-coarse sand layer containing large clasts, that are present throughout the terrace. (D) Lower section of T3. (E) Micro-ripples on thin beds in Lower Terrace. (F) Outcrop of the lower section of T3, showing predominantly scoured thin-bedded deposition. (G) Upper section of T3, characterised by increased bed thicknesses, with beds exhibiting lateral accretion, and hummock-like geometries.

Figure 8. Sedimentary log through the lower and upper sections of T3, showing change in grainsize, bed thickness and bed geometries. The lower section of the terrace is characterised by six packages of thickening and coarsening up beds. In contrast, the upper terrace is characterised by a lack of discernible bed thickness and grainsize trends but exhibits a higher degree of erosion and greater bed thicknesses.

Figure 9. Stratigraphic evolution of succession studied at La Peña. (A) Deposition of Package 1 and T1 is followed by (B) over-spilling onto an MTD palaeohigh, and partial erosion of T1 by the base of Package 2, before the initiation of channelised bodies, and concurrent lateral migration. Possible development of T2 and T3. (C) Package 3 is characteried by a return to deposition of tabular geometries, and further development of T2 and T3. (D) The start of Package 4 deposition is characterised by repeated deposition of ponded and lobate beds, and erosion of these features by a small channel to the west. This is followed by repeated deposition of lobe and hybrid beds.

Figure 10. Summary of S1 and axial channel-fill. (A) Incisional avulsion, where S1 is formed contemporaneously with depositional systems. (B) The NSB and SSB represent coetaneous exit channels from a mini-basin, with the NSB having a lower thalweg gradient. The high gradient in the SSB causes total bypass of flows, with deposition in the NSB. Once aggradation within the NSB exceeds the generation of accommodation, flows are transported down the SSB, which subsequently back-fills.

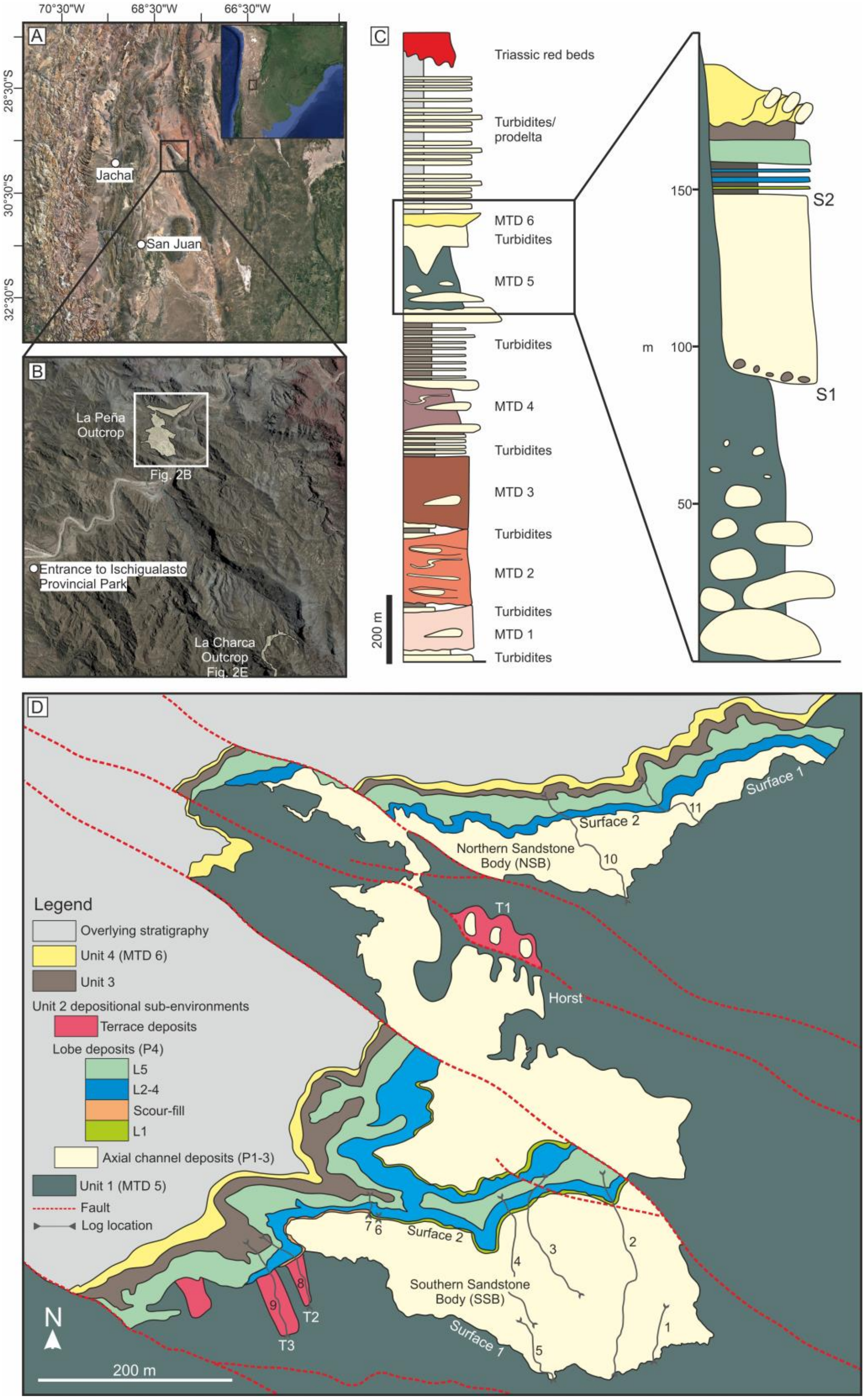

70°30"W
68°30"W
66°30"W
28°30"S
30°30"S
32°30"S
A
Jachal
San Juan
B
La Peña Outcrop
Fig. 2B
Entrance to Ischigualasto Provincial Park
La Charca Outcrop Fig. 2E
C
Triassic red beds
Turbidites/ prodelta
MTD 6
Turbidites
MTD 5
Turbidites
MTD 4
Turbidites
MTD 3
Turbidites
MTD 2
Turbidites
MTD 1
Turbidites
200 m
m
150
100
50
S2
S1
D
Surface 1
Surface 2
Northern Sandstone Body (NSB)
T1
Horst
Southern Sandstone Body (SSB)
T2
T3
Legend
Overlying stratigraphy
Unit 4 (MTD 6)
Unit 3
Unit 2 depositional sub-environments
Terrace deposits
Lobe deposits (P4)
L5
L2-4
Scour-fill
L1
Axial channel deposits (P1-3)
Unit 1 (MTD 5)
Fault
Log location
N
200 m

Figure 1

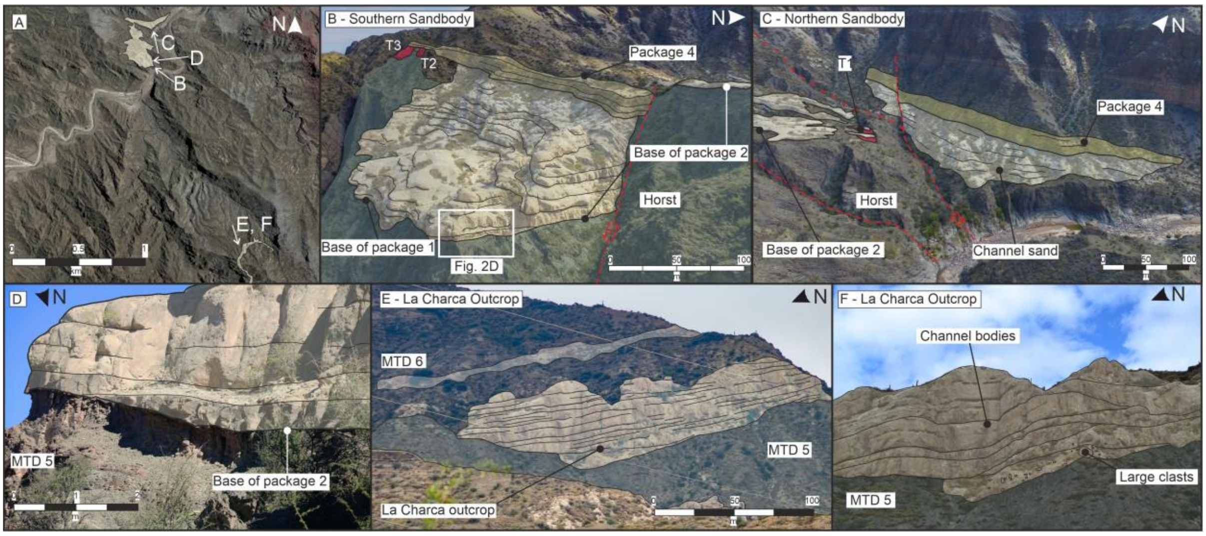
A
N
C
D
B
E, F
B - Southern Sandbody
N
T3
T2
Package 4
Base of package 2
Horst
Base of package 1
Fig. 2D
C - Northern Sandbody
N
T1
Package 4
Horst
Base of package 2
Channel sand
D
N
MTD 5
Base of package 2
E - La Charca Outcrop
N
MTD 6
MTD 5
La Charca outcrop
F - La Charca Outcrop
N
Channel bodies
Large clasts
MTD 5

Figure 2

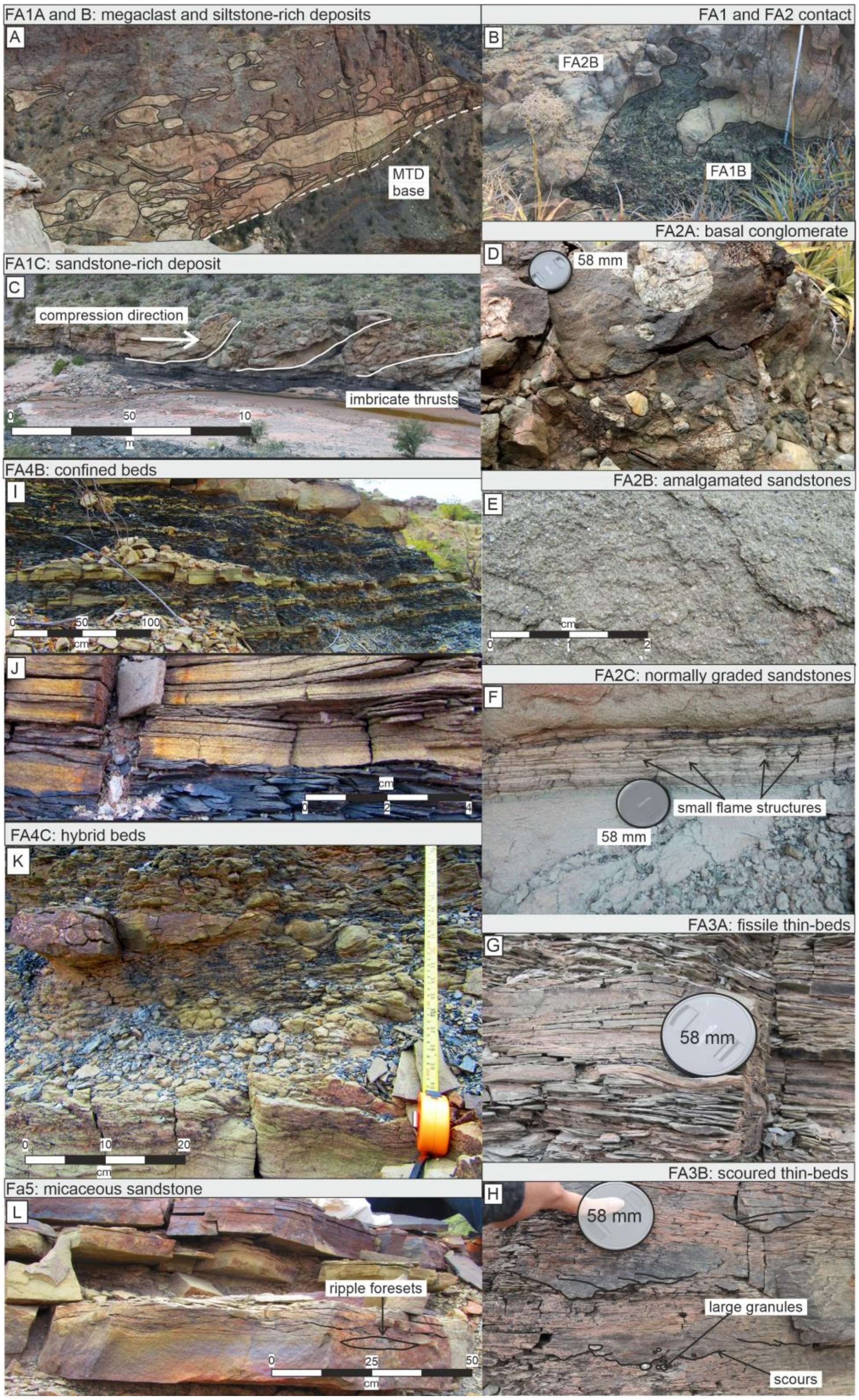
FA1A and B: megaclast and siltstone-rich deposits
A
MTD base
FA1 and FA2 contact
B
FA2B
FA1B
FA2A: basal conglomerate
D
58 mm
FA1C: sandstone-rich deposit
C
compression direction
imbricate thrusts
0
50
10
m
FA2B: amalgamated sandstones
E
cm
0
1
2
FA4B: confined beds
I
0
50
100
cm
J
cm
0
2
4
FA2C: normally graded sandstones
F
small flame structures
58 mm
FA4C: hybrid beds
K
0
10
20
cm
FA3A: fissile thin-beds
G
58 mm
Fa5: micaceous sandstone
L
ripple foresets
0
25
50
cm
FA3B: scoured thin-beds
H
58 mm
large granules
scours

Figure 3

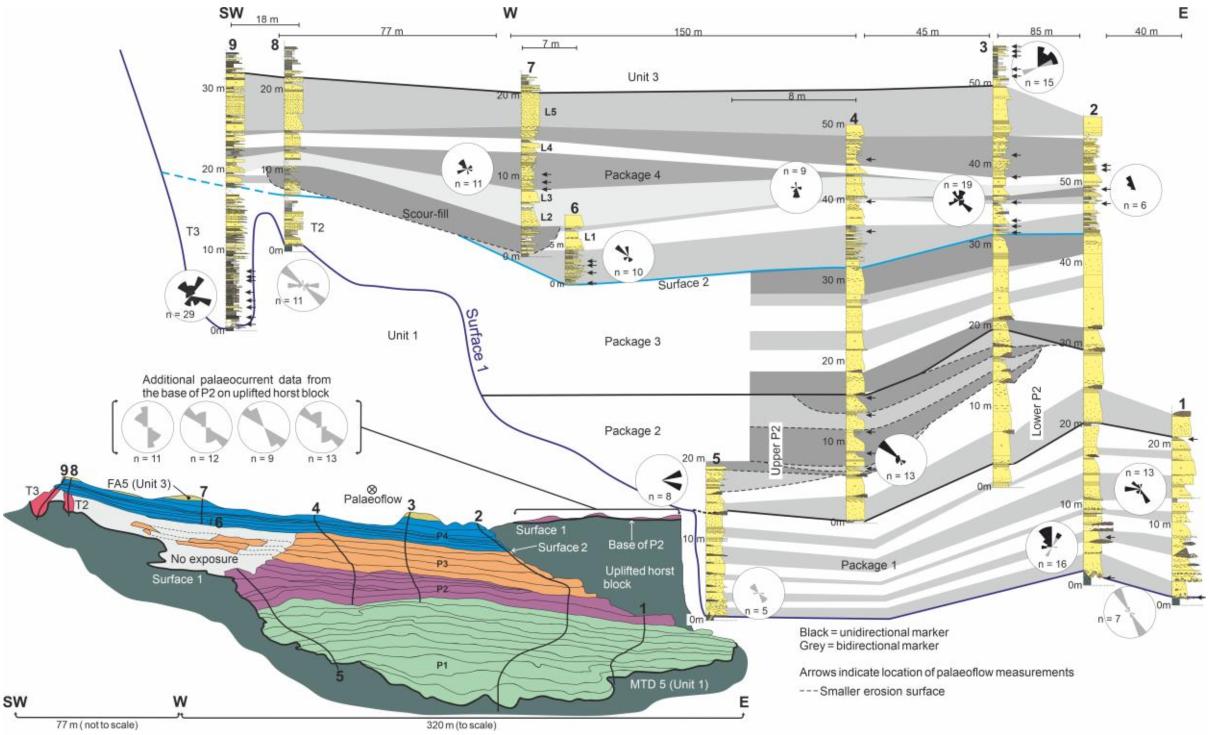
SW
W
E
18 m
77 m
7 m
150 m
8 m
45 m
85 m
40 m
Unit 3
Package 4
Scour-fill
Surface 2
Unit 1
Surface 1
Package 3
Package 2
Package 1
Upper P2
Lower P2
T3
T2
L1
L2
L3
L4
L5
Additional palaeocurrent data from the base of P2 on uplifted horst block
n = 11
n = 12
n = 9
n = 13
n = 29
n = 11
n = 10
n = 8
n = 5
n = 19
n = 15
n = 6
n = 16
n = 7
FA5 (Unit 3)
Palaeoflow
No exposure
Surface 1
Surface 2
Base of P2
Uplifted horst block
P4
P3
P2
P1
MTD 5 (Unit 1)
77 m (not to scale)
320 m (to scale)
Black = unidirectional marker
Grey = bidirectional marker
Arrows indicate location of palaeoflow measurements
Smaller erosion surface

Figure 4

Figure 5

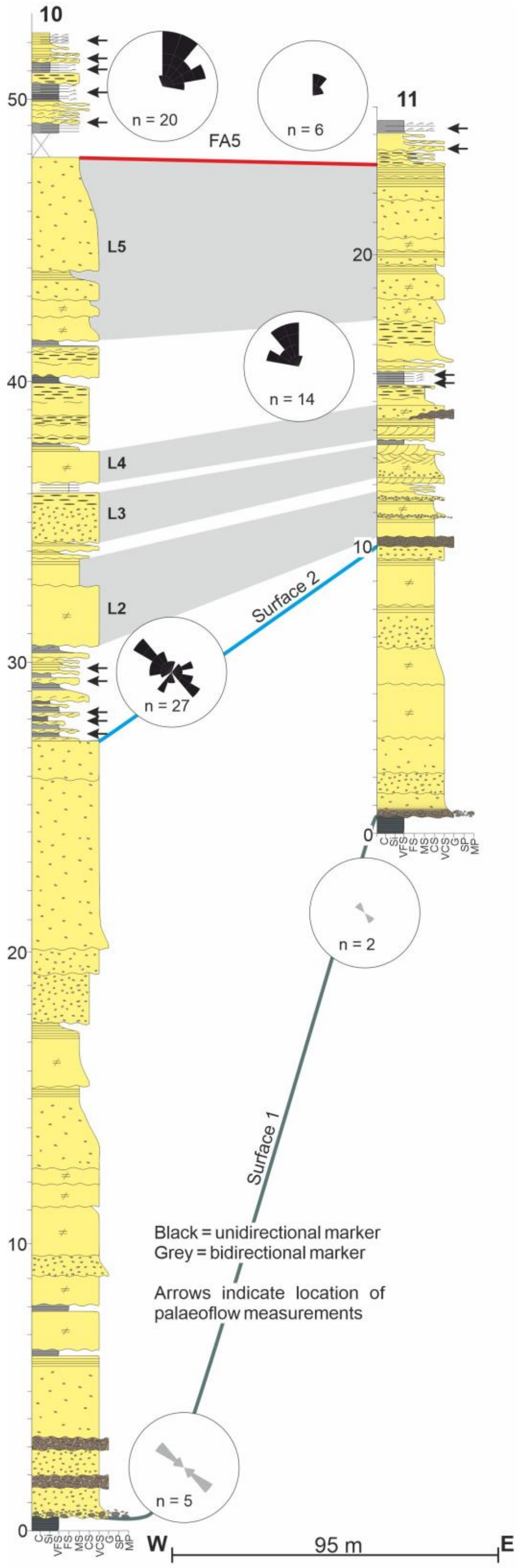

1360

1361 Figure 6

1362

1363

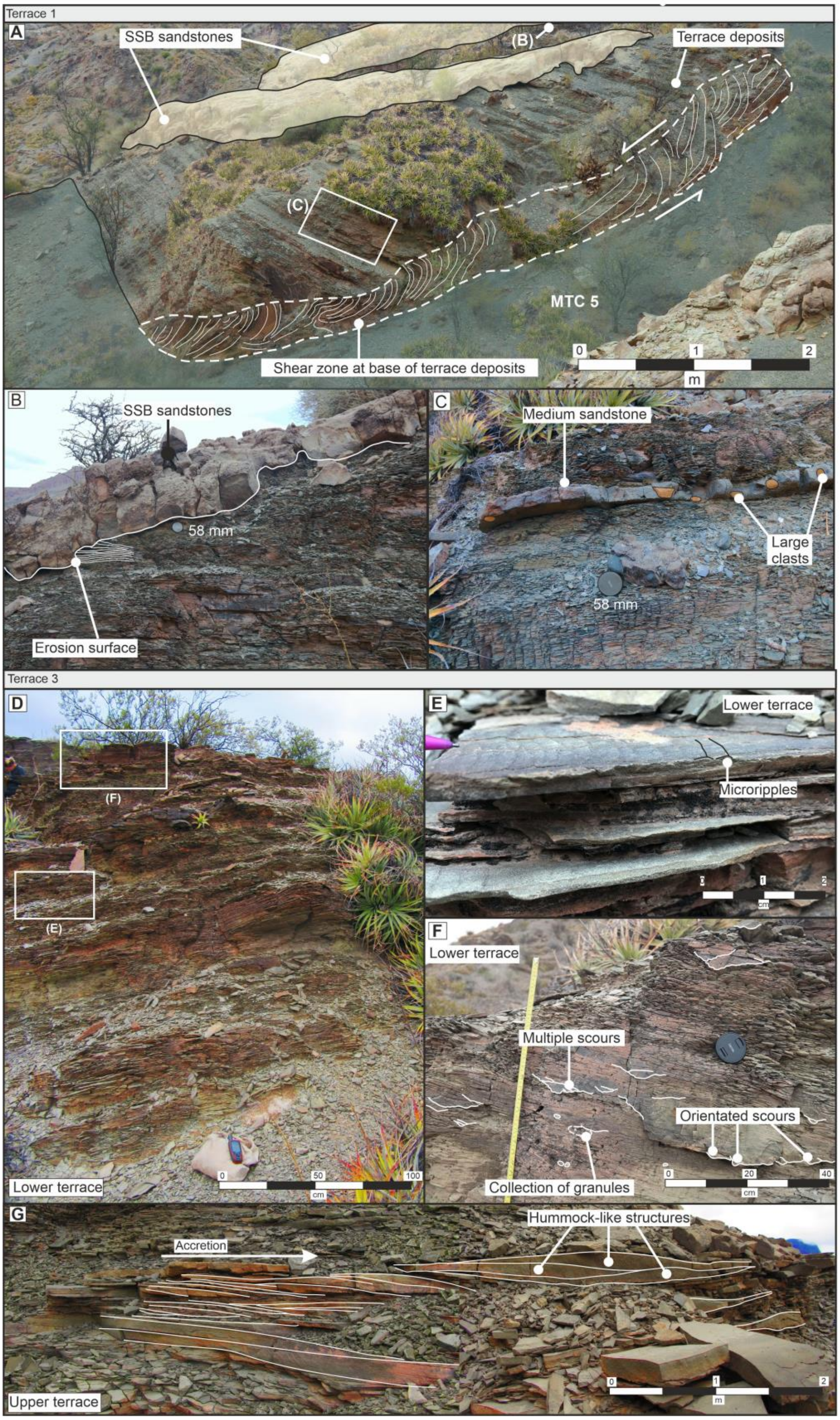

1364 Figure 7

1365

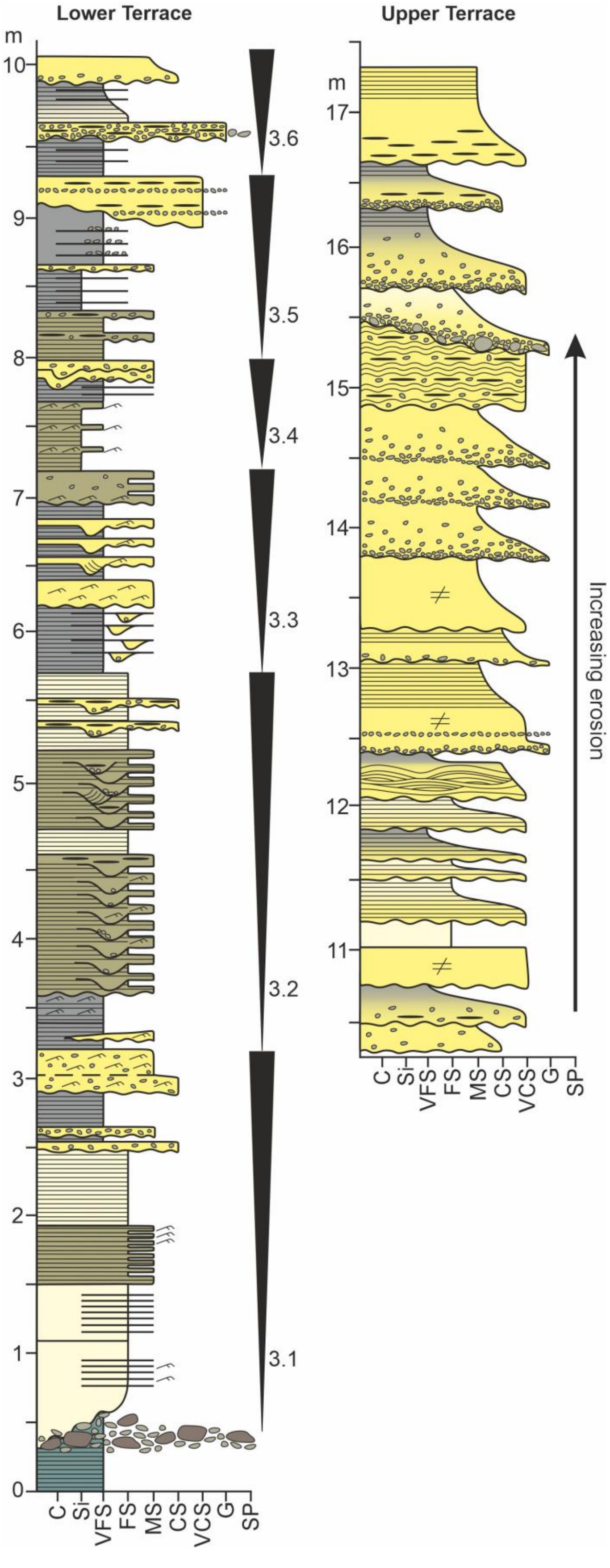

1366 Figure 8

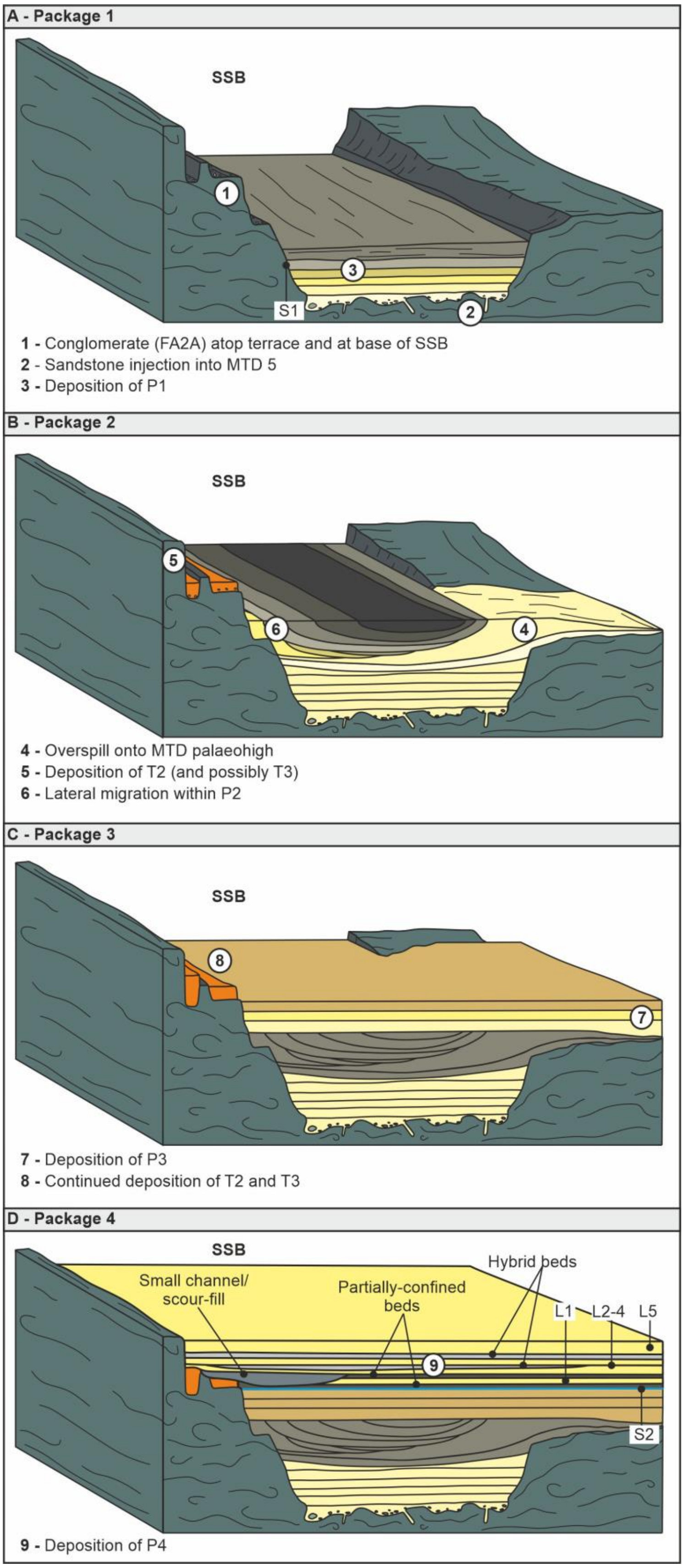
A - Package 1
SSB
S1
1 - Conglomerate (FA2A) atop terrace and at base of SSB
2 - Sandstone injection into MTD 5
3 - Deposition of P1
B - Package 2
SSB
4 - Overspill onto MTD palaeohigh
5 - Deposition of T2 (and possibly T3)
6 - Lateral migration within P2
C - Package 3
SSB
7 - Deposition of P3
8 - Continued deposition of T2 and T3
D - Package 4
SSB
Small channel/
scour-fill
Partially-confined
beds
Hybrid beds
L1
L2-4
L5
S2
9 - Deposition of P4

Figure 9

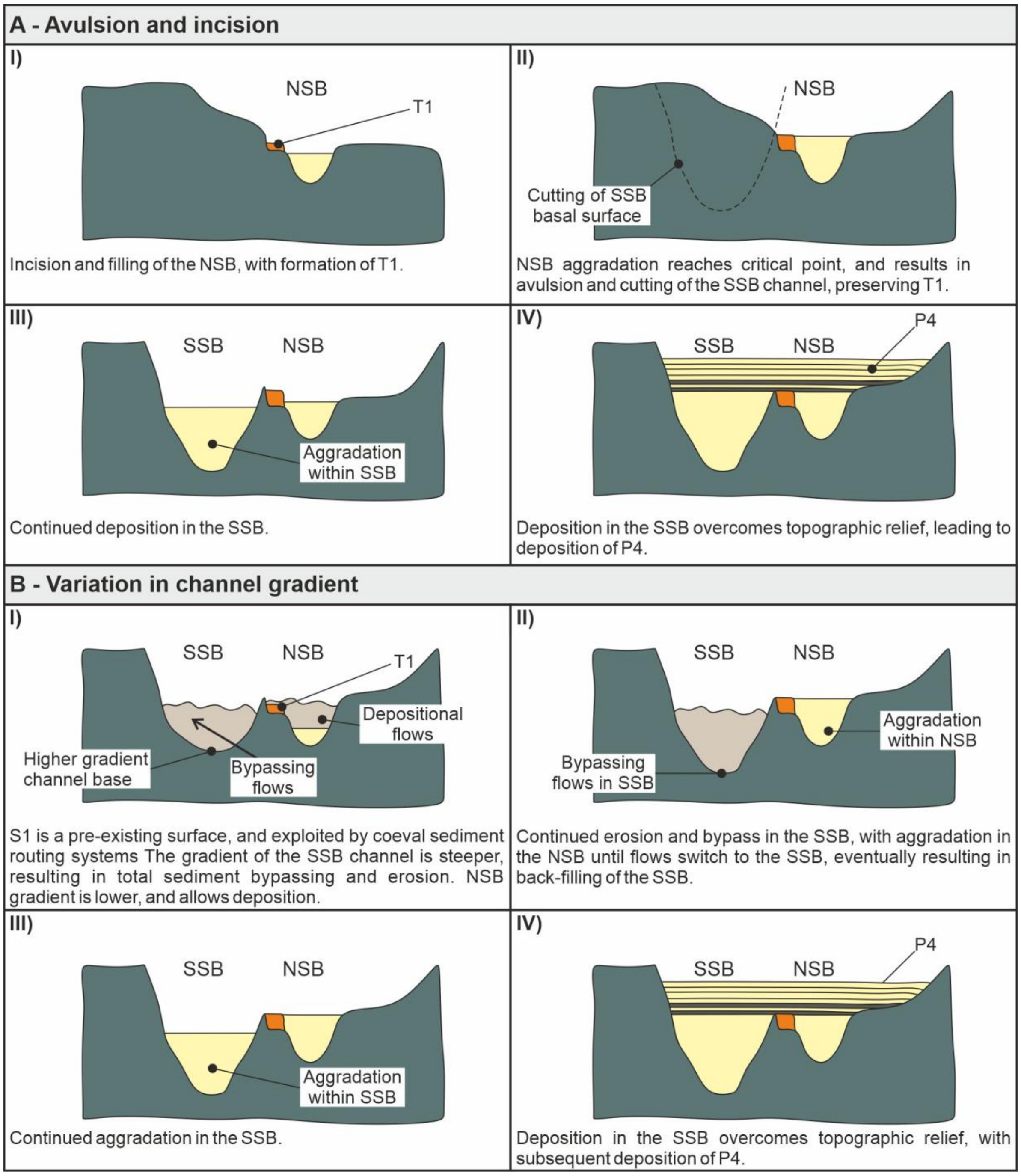

Figure 10

END